Cannabinoids promote NREM sleep via inhibition of prefrontal cortico-hypothalamic projections

Xufeng Xu

Qingdao University

Haixing Zhong

Fourth Military Medical University

Huamin Xu

Qingdao University

Xin Li

Fourth Military Medical University

Rou-gang Xie

Fourth Military Medical University

Ying Wang

Qingdao University   https://orcid.org/0000-0003-4616-031X

Li Tong

Chinese PLA General Hospital

Qianqian Zhu

Qingdao University

Junxia Xie

Qingdao University

Jing Han

Shaanxi Normal University

Li Zhang

University of Southern California

Zhian Hu

Third Military Medical University

Ning Gu

ning.gu@mcgill.ca

Hailong Dong

Fourth Military Medical University   https://orcid.org/0000-0001-8984-9067

Xia Zhang (✉ Xia.Zhang@theroyal.ca)

University of Ottawa

Article

Cannabinoids promote NREM sleep via inhibition of prefrontal cortico-hypothalamic projections

Xufeng Xu,[1,2,9] Haixing Zhong,[3,9] Huamin Xu,[1,2,9] Xin Li,[3] Rou-gang Xie,[3] Ying Wang,[1] Li Tong,[4] Qianqian Zhu,[1] Junxia Xie,[1] Jing Han,[5] Li Zhang,[6] Zhian Hu,[7] Ning Gu,[8]* Hailong Dong,[3]* Xia Zhang[1,2,3,5,10]*

[1]Institute of Brain Science and Disease, Qingdao University, No. 308, Ningxia Road, Qingdao, 266071, China. [2]University of Ottawa Institute of Mental Health Research at the Royal, 1145 Carling Avenue, Ottawa, K1Z7K4, Canada. [3]Department of Anesthesiology and Perioperative Medicine, Xijing Hospital, Fourth Military Medical University, Xi'an, 710032, China. [4]Anesthesia and Operation Center, Chinese PLA General Hospital, Beijing, 100853 China. [5]Key Laboratory of Modern Teaching Technology & College of Life Sciences, Shaanxi Normal University, Xian, 710062, China. [6]Zilkha Neurogenetic Institute, Keck School of Medicine, University of Southern California, Los Angeles, CA90033, USA. [7]Department of Physiology, Collaborative Innovation Center for Brain Science, Third Military Medical University, Chongqing 400038, China. [8]Department of Physiology, McGill University, 3655 Prom. Sir-William-Osler, Montreal, H3G1Y6, Canada.

[9]These authors contributed equally to this work

[10]Lead Contact

*Corresponding author. Email: Xia.Zhang@theroyal.ca (X.Z.), hldong6@hotmail.com (H.D.) or Ning.Gu@theroyal.ca

Cannabinoids promote non-rapid eye movement (NREM) sleep, but its underlying mechanism is not known. Here we find that cannabinoid promotion of NREM sleep is inhibited by cannabinoid antagonist injection systemically or into the dorsomedial hypothalamus (DMH), where cannabinoids selectively inhibit glutamatergic inputs synapsing with glutamatergic but not GABAergic neurons. Photoactivation of DMH-projecting ventromedial prefrontal cortical (vmPFC) neurons, their terminals, or their postsynaptic DMH neurons rapidly switches NREM sleep to wakefulness, which is blocked by photoinhibition of DMH outputs. Chemoactivation of DMH glutamatergic but not GABAergic neurons innervated by vmPFCs promotes wakefulness and suppresses NREM sleep, whereas chemoinhibition of vmPFC projections in DMHs produces opposite effects by mimicking cannabinoid effects. DMH-projecting vmPFC neurons are inhibited during NREM sleep and activated during wakefulness. Chemoactivation of DMH-projecting vmPFC neurons blocks cannabinoid promotion of NREM sleep and suppression of wakefulness. Thus, vmPFC neurons innervating DMHs represent the first identified set of cerebral cortical neurons for promotion of physiological wakefulness and suppression of NREM sleep, while cannabinoid inhibition of vmPFC projections in DMHs promotes NREM sleep and suppresses wakefulness.

Long-term sleep problems, which affect 25-30% of human population[1], is associated with profound health problems, including anxiety, depression, cardiovascular disorders, and obesity[1,2]. Sleep-wake states consist of rapid eye movement (REM) sleep, non-REM (NREM) sleep and wakefulness. Preclinical studies showed that synthetic cannabinoids Δ9-tetrahydrocannabinol (THC) and WIN55,212-2 promoted NREM sleep and suppressed wakefulness[3,4]. While cannabis withdrawal in humans caused sleep problems[5], synthetic cannabinoids promoted human NREM sleep[6] and improve sleep quality and sleep disturbances[7-10]. However, the exact mechanisms underlying cannabinoid modulation of sleep are not known[10].

Experimental activation of sleep-promoting cells in the hypothalamus, basal forebrain and brainstem switches wakefulness to sleep[2,11-13]. In 1920s, von Economo indicated the midbrain and posterior hypothalamus to regulate wakefulness[14]. It is now known that main wake-promoting cells are located in the brainstem, hypothalamus, and basal forebrain[11-13,15,16] and their activation promotes wakefulness through ascending projections to cerebral cortices[2,12,13]. After nearly a century of intensive and extensive sleep study, however, it remains unknown whether cerebral cortices, as the center of the central nervous system to process high-order information, contain wake-promoting cells.

In this study, we employed in vivo sleep recording, neurophysiology, the cutting-edge neuroanatomical sparse labeling, conditional mouse mutagenesis, opto/chemogenetic strategy, and in vivo calcium imaging to investigate the mechanism underlying cannabinoid modulation of sleep-wake behavior. Surprisingly, we found an unanticipated cerebrohypothalamic pathway linking not only activation of ventromedial prefrontal cortical (vmPFC) projections in the dorsomedial hypothalamus (DMH), promotion of wakefulness and suppression of NREM sleep,

3

but also cannabinoid inhibition of vmPFC projections in the DMH, promotion of NREM sleep and suppression of wakefulness.

Results

Cannabinoid modulation of sleep-wake behavior

Because rodents sleep in the day, we injected synthetic cannabinoids 10-30 min before lights-on (8:00 AM) and analyzed electroencephalogram (EEG) and electromyogram (EMG) recordings. We first examined detailed changes of sleep-wake states after administration of nabilone, a synthetic cannabinoid currently licensed as Cesamet in Canada for the treatment of chemotherapy-associated nausea and vomiting. Nabilone (0.2, 1, 5 mg/kg, i.p.) dose-dependently promoted NREM sleep and suppressed both wakefulness and REM sleep (Fig. 1a-c) for over 12 h (Fig. 1d-f). Specifically, the moderate dose of nabilone (1 mg/kg, i.p.) promoted NREM sleep from approximately 58% of the baseline sleep-wake state to 85% and suppressed wakefulness and REM sleep from approximately 33% and 9% to 13% and 2%, respectively (Fig. 1a-c). EEG hypnograms also showed significant changes of sleep and wake architecture after nabilone administration (Fig. 1g). Nabilone significantly increased bout duration but not number of NREM sleep, decreased bout duration but not number of wakefulness, and decreased both bout number and duration of REM sleep (Fig. 1h-m). HU210 (5, 10, 20, 50 μg/kg, i.p.), the most potent synthetic cannabinoid, also dose-dependently promoted NREM sleep and suppressed both wakefulness and REM sleep (Extended Data Fig. 1a-c).

To examine whether cannabinoids modulate sleep via the CB_1 cannabinoid receptor (CB_1R), we conducted both systemic and intra-cerebral injection of the CB_1R antagonist AM281 (2 mg/kg, i.p.; 50 ng/0.2 μl, intra-cerebral injection)[17,18]. Systemic injection of AM281 but not

vehicle, which did not significantly affect sleep-wake states on its own, significantly inhibited the effects of nabilone on NREM sleep and wakefulness without significant effects on cannabinoid suppression of REM sleep (Extended Data Fig. 1d-f). The DMH is a central hub for modulation of sleep-wake states[12,13,19,20], ingestion, reproduction, endocrine, cardiovascular function, respiration, and thermogenesis[21-23]. We therefore examined the possible DMH location of systemic cannabinoid modulation of sleep-wake states. Bilateral intra-DMH injection of AM281 (Extended Data Fig. 1g,h), which did not significantly affect sleep-wake behavior on its own, significantly inhibited the effects of nabilone on NREM sleep and wakefulness without significant effects on cannabinoid suppression of REM sleep (Extended Data Fig. 1i-k). These results suggest that cannabinoids activate DMH CB$_1$R to promote NREM sleep and suppress wakefulness.

Cannabinoids deactivate DMH glutamatergic but not GABAergic neurons

We next performed patch clamp experiments on hypothalamic slices to explore whether cannabinoids act on DMH presynaptic CB$_1$R of GABAergi, glutamatergic or both synapses. Endocannabinoids specifically mediate depolarization-induced suppression of inhibition (DSI) or excitation (DSE) at GABAergic or glutamatergic synapses, respectively, through activation of GABAergic or glutamatergic presynaptic CB$_1$R, respectively[24,25]. DMH neurons with or without low-threshold spikes (LTS) were known as LTS(+) or LTS(-) neurons, respectively[26]. With whole-cell patch clamp on hypothalamic slices, we found that application of nabilone did not significantly affect DSI recorded from LTS(-) and LTS(+) neurons (Fig. 2a,b,i). However, nabilone significantly inhibited DSE at glutamatergic inputs onto DMH LTS(-) neurons (Fig. 2c,i) but not LTS(+) neurons (Fig. 2d,i). While the DMH contains both GABAergic and glutamatergic

5

neurons[20], we used two types of GABA and glutamate mutant mice to reveal that LTS(+) and

LTS(-) DMH neurons were GABAergic and glutamatergic neurons, respectively (see Methods).

HU210 did not significantly change DSE of DMH GABAergic neurons (Fig. 2e,i), but nabilone

significantly inhibited DSE of DMH glutamatergic neurons (Fig. 2f,i). Because activation of

glutamatergic presynaptic CB_1R inhibits presynaptic release of glutamate, producing

deactivatory (i.e., inhibitory) effects on postsynaptic neurons[24,25], it was not surprised to find that

bath application of nabilone significantly reduced firing rates of DMH LTS(-) but not LTS(+)

neurons (Fig. 2g-i). Our results together suggest that cannabinoids selectively activate CB_1R at

DMH glutamatergic but not GABAergic inputs synapsing with DMH glutamatergic but not

GABAergic neurons, leading to sequential inhibition of DMH glutamatergic inputs and

glutamatergic neurons.

Mapping brain regions innervated by DMH-projecting vmPFC neurons

Then, which brain region sends glutamatergic inputs to the DMH for modulation of sleep-wake

behavior? The vmPFC, i.e., the prelimbic, infralimbic and dorsal preduncular subregions in

rodents, is a central hub that controls multiple brain regions through its internal circuitry and

external connectivity[27-31]. The vmPFC plays a key role in decision-making, value-coding,

thinking and emotional arousal/recognition[30,32] and sends glutamatergic projections into the

DMH in rats[33]. Therefore, the vmPFC may actively participate in modulation of sleep-wake

behavior through its glutamatergic projections in the DMH. We then conducted neuroanatomical

tract-tracing experiments to investigate glutamatergic vmPFC-DMH projections in detail. In

mice injected with the retrograde-tracing virus pAAV-SYN-MCS-mCherry-3FLAG into the

DMH (Fig. 3a,b), we observed mCherry-labeled neurons specifically in the 5th layer of the vmPFC (Fig. 3c), which is in agreement with a recent study on rats[33].

It is known that the vmPFC projects to multiple brain regions[27-31], but it is not clear if the same vmPFC neuron innervating the DMH also project to major brain regions of sleep- and wake-promoting. Employing the recently developed sparse labelling approach[34], we injected the rAAV2-Camk2-mCherry-2A-Cre into the DMH, which was transported back to vmPFC cell bodies and turned on the Cre-dependent virus mixture of both controller (pAAV-TRE-DIO-FLPo) and amplifier vectors (pAAV-TRE-fDIO-GFP-IRES-Tta) injected into the ipsilateral vmPFC (Fig. 3d). After vectors containing the bright EGFP were transported and labelled the whole vmPFC neuron, including its axons and terminals, mice were killed for clearing of the whole brain[35], followed by imaging of the brain with a light sheet microscope. DMH-projecting vmPFC neurons showed their entirety with cell bodies located in the vmPFC and their axons projecting all the way downward and caudalward into the rAAV2-Camk2-mCherry-2A-Cre injection site in the DMH but not its surrounding regions (Fig. 3e-g), confirming the validity of our target-specific labeling strategy. Along their way toward the DMH, axons sent collaterals heavily innervating the nucleus accumbens (Fig. 3h), which is the only brain region receiving as highest terminal innervation as the DMH. Moderate density of axonal terminals was found in the motor cortex, anterior cingulate cortex, bed nuclei of the stria terminalis (Fig. 3i), preoptic hypothalamus and anterior hypothalamus (Fig. 3i), with low density in the bottom part of the thalamus. While the preoptic hypothalamus contains sleep-promoting neurons[11-13], we did not detect axons/terminals in the wake-promoting paraventricular thalamus (PVT), lateral hypothalamus (LH), tuberomammillary nucleus, basal forebrain, ventral tegmental area (VTA), raphe nuclei, locus coeruleus (LC), and parabrachial nucleus[11].

7

In order to examine whether the results obtained with sparse labeling approach are reliable, we conducted another experiment for double labeling of vmPFC neurons innervating the DMH and PVT. Mice received an injection of retrograde-tracing virus pAAV-SYN-MCS-mCherry-3FLAG into the DMH and pAAV-SYN-MCS-EGFP-3FLAG into the PVT (Fig. 3j-l). Almost all DMH-projecting neurons are located in the layer 5 of the vmPFC, whereas PVT-projecting neurons are mainly located in the layer 6 with a few cells in the lay 5, which did not show double labeling with DMH-projecting neurons (Fig. 3m). These results clearly reveal that although vmPFC neurons directly innervate both the DMH and PVT, DMH-projecting vmPFC neurons do not project to the PVT, thus confirming our sparse labeling results.

Optoactivation of vmPFC-DMH projections switches NREM sleep to wakefulness

While we observed that intra-DMH injection of the CB_1R antagonist AM281 inhibited cannabinoid promotion of NREM sleep and suppression of wakefulness, we also found that cannabinoids selectively inhibited glutamatergic inputs in the DMH. We reasoned that if inhibition of DMH glutamatergic inputs participated in cannabinoid promotion of NREM sleep and suppression of wakefulness, activation of DMH inputs would promote wakefulness and suppress NREM sleep. As neurons in the 5th layer of the vmPFC directly innervated the DMH (Fig. 3), we hypothesized that in contrast to inhibitory effects of cannabinoids on vmPFC-DMH projections, activation of vmPFC-DMH glutamatergic projections may promote wakefulness and suppress NREM sleep. To examine the hypothesis, we employed optogenetic strategy to activate DMH-projecting vmPFC neurons with adeno-associated virus (AAV) expressing channelrhodopsin 2 (ChR2). We injected the pseudorabies virus vector expressing Cre recombinase (PRV-Cre)[36] into bilateral DMHs for transport of Cre back to cell bodies in the

vmPFC, followed 5 weeks later by an injection of AAV-Camk2-DIO-ChR2-mCherry (or AAV-Camk2-DIO-mCherry as control) into bilateral vmPFCs (Fig. 4a). Mice receiving both PRV-Cre and AAV-Camk2-DIO-ChR2-mCherry were killed for patch clamp experiments on brain slices. We applied blue laser light stimulation of 1, 10, 20 or 50 Hz (5 mW, 10 ms each pulse, 10 sec total) to red fluorescence mCherry-labelled cells in the 5th layer of the vmPFC. Photostimulation produced frequency-dependent increase of spiking up to 20 Hz (Extended Data Fig. 2), suggesting not only a specific transgene expression of ChR2 in glutamatergic vmPFC neurons innervating the DMH but also their activation by photostimulation.

Because 10-Hz photostimulation reliably activated layer-5 neurons in the vmPFC[30] (Extended Data Fig. 2), we used both 1- and 10-Hz to assess ChR2 function in real-time mice. Each mouse received at least 3 trains of 1-Hz and 10-Hz stimuli for 10 sec with 40-60 min interval between each train. The same photostimulation protocol was used for activation purpose throughout all experiments in this study. In mice receiving AAV-Camk2-DIO-ChR2-mCherry but not AAV-Camk2-DIO-mCherry within bilateral vmPFCs together with PRV-Cre injection confined to bilateral DMHs (Fig. 4d and Extended Data Fig. 3a,e), photostimulation of 10 Hz but not 1 Hz switched NREM sleep to wakefulness in approximately 3 sec after the onset of the first stimulation (Fig. 4g,j and Extended Data Movie S1). Photostimulation significantly increased the probability of wakefulness, together with a complementary decrease of NREM but not REM sleep probability (Fig. 4m-o). However, the same photostimulation of neither 1 Hz nor 10 Hz during REM sleep wakened the same mice (Extended Data Fig. 4a,d and Movie S2).

In principle, photostimulation of vmPFC neurons innervating DMHs could activate other brain regions directly innervated by the same vmPFC neurons. To overcome this potential problem, we tried to activate vmPFC outputs in DMHs. Following AAV-Camk2-ChR2-mCherry

9

(or AAV-Camk2-mCherry as control) injection into bilateral vmPFCs, a pair of optic fibers were implanted above bilateral DMHs at 40° oralward angle (Fig. 4b). After EEG/EMG recording, mice with virus injection confined to bilateral vmPFCs showed mCherry-labeled glutamatergic vmPFC neurons and their axon terminals in DMHs (Fig. 4e and Extended Data Fig. 3b). In mice receiving AAV-Camk2-ChR2-mCherry but not AAV-Camk2-mCherry within bilateral vmPFCs (Extended Data Fig. 3b), photostimulation of DMHs with 10 Hz but not 1 Hz switched NREM sleep to wakefulness in approximately 3 sec after the onset of the first stimulation (Fig. 4h, k). Neither 1-, 10- or 20-Hz photostimulation nor a series of 10- and 20-Hz photostimuli during REM sleep wakened the same mice (Extended Data Fig. 4b,e,g). Interestingly, photostimulation of 10 or 20 Hz during wake phase did not produce significant effects (Extended Data Fig. 4c,f).

Activation of axon terminals in DMHs may lead to back-propagating action potentials to produce an antidromic activation of vmPFC cell bodies, leading to activation of other brain regions directly innervated by these vmPFC neurons. To overcome this potential problem, we tried to activate DMH neurons innervated by vmPFC projections. We recently showed that pAAV-Cre from transduced neurons was transported to their axon terminals for an effective and specific driving of Cre-dependent transgene expression in selected postsynaptic neurons[37]. Accordingly, we injected pAAV-hSyn-EGFP-2A-Cre into bilateral vmPFCs, and 5 weeks later pAAV-EF1a-DIO-ChR2-mCherry (or pAAV-EF1a-DIO-mCherry as control) was injected into bilateral DMHs, followed by implantation of a pair of optic fibers above bilateral DMHs at 40° oralward angle (Fig. 4c). In mice receiving pAAV-EF1a-DIO-ChR2-mCherry but not pAAV-EF1a-DIO-mCherry within bilateral DMHs and pAAV-hSyn-EGFP-2A-Cre confined in bilateral vmPFCs (Fig. 4f and Extended Data Fig. 3c,f), photostimulation of 10 Hz but not 1 Hz also switched NREM sleep to wakefulness in approximately 3 sec (Fig. 4i, l), thus mimicking

wakening effects produced by photoactivation of vmPFC cell bodies and their axon terminals innervating DMHs. These findings strongly suggest that optoactivation of vmPFC-DMH projections rapidly switches NREM but not REM sleep to wakefulness .

Delta waves (1-4 Hz) are characteristics of NREM sleep, while theta waves (4-8 Hz) appear in both REM sleep and wakefulness that also includes alpha waves (8-14 Hz), beta waves (14-30 Hz) and gamma waves (30-100 Hz) [2,16]. We analyzed EEG brain waves before, during and after photostimulation in mice receiving photostimulation of postsynaptic DMH neurons of vmPFC-DMH projections (Fig. 4c). Photostimulation significantly increased the power of alpha, beta, gamma and total waves (1-100 Hz) without significant effects on the power of delta and theta waves (Extended Data Fig. 5), suggesting the power of driving to wakefulness.

While photostimulation of DMH glutamatergic inputs from the 5th layer of the vmPFC switched NREM sleep to wakefulness, we next examined if application of the same photostimulation protocol to PVT glutamatergic inputs from the 6th layer of the vmPFC could switch NREM sleep to wakefulness. After injection of AAV-Camk2-ChR2-mCherry injection (or AAV-Camk2-mCherry as control) into bilateral vmPFCs, an optic fiber was implanted 0.05 mm above the PVT at 45° cardalward angle and 10° towards the midline (Extended Data Fig. 6a). In mice with virus injection within the bilateral vmPFCs (Extended Data Fig. 6b), neither 1- nor 10-Hz photostimulation of the PVT wakened mice from NREM sleep (Extended Data Fig. 6c,d). Nevertheless, application of the same photostimulation of 10-Hz but not 1-Hz to the PVT switched NREM sleep to wakefulness in approximately 10 sec after the onset of the first stimulation (results not shown), thus confirming a recent study[38].

Chemoactivation of DMH glutamatergic but not GABAergic neurons innervated by vmPFCs promotes wakefulness and suppresses NREM sleep

As the DMH contains glutamatergic neurons[20], we examined the effects on sleep-wake states of activation of DMH glutamatergic neurons innervated by the vmPFC. We employed our vGlut2-iCreERT2 mutant mice[36] and transsynaptic tagging strategy[37] for a specific transgene expression in DMH glutamatergic neurons innervated by vmPFCs. Instead of employing optogenetic strategy, here we utilized chemogenetic strategy for a stable activation of neurons for several hours, during which changes of sleep-wake states could be assessed after a clozapine-N-oxide (CNO) injection at 10:00 am, a time approximating peak sleep drive in mice. Mice received pAAV-hSyn-DIO-EGFP-T2A-NLS-Flipo injection into bilateral vmPFCs, followed 5 weeks later by pAAV-EF1a-fDIO-hM3Dq-mCherry (or pAAV-EF1a-fDIO-mCherry as control) injection into bilateral DMHs (Fig. 5a). Patch clamp recording of mCherry-labeled DMH neurons revealed a significant increase in their firing rates after bath application of CNO onto hypothalamic slices (Fig. 5b), suggesting both successful Cre-dependent transgene expression in and CNO-elicited activation of DMH glutamatergic neurons innervated by vmPFCs. In mice receiving pAAV-EF1a-fDIO-hM3Dq-mCherry, but not pAAV-EF1a-fDIO-mCherry, within bilateral DMHs together with pAAV-hSyn-DIO-EGFP-T2A-NLS-Flipo confined in bilateral vmPFCs (Fig. 5c and Extended Data Fig. 3d,g), CNO (0.5 mg/kg, i.p.) but not vehicle injection significantly promoted wakefulness and suppressed NREM sleep without significant effects on REM sleep (Fig. 5d,e). The CNO-induced promotion in wakefulness was primarily due to longer wake bouts and less number of wake bouts (Fig, 5f), suggesting an efficient promotion of wakefulness after activation of vmPFC-DMH projections. The promotion in wakefulness across

12

12h in light phase was followed by insignificant changes of sleep-wake states across 12h in darker phase (Extended Data Fig. 7).

As the DMH also contains GABAergic neurons[20], we further employed chemogenetic strategy to examine the effects on sleep-wake states following activation of DMH GABAergic neurons innervated by vmPFCs. We used Dlxa-Cre mice carrying Cre in forebrain GABAergic neurons used in our recent study[39]. Mice received pAAV-hSyn-DIO-EGFP-T2A-NLS-Flipo injection into bilateral vmPFCs, followed 5 weeks later by pAAV-EF1a-fDIO-hM3Dq-mCherry (or pAAV-EF1a-fDIO-mCherry as control) injection into bilateral DMHs (Extended Data Fig. 8a). In mice with virus injection within bilateral vmPFCs and DMHs, a CNO injection (0.5 mg/kg, i.p.) at 10:00 am did not produce significant effects on sleep-wake states (Extended Data Fig. 8b-f). Our results together suggest that activation of glutamatergic but not GABAergic neurons innervated by vmPFCs promotes wakefulness and suppresses NREM but not REM sleep.

NREM switch to wakefulness by optoactivation of DMH-projecting vmPFC neurons is blocked by optoinhibition of DMH outputs in LHs

While DMH glutamatergic neurons mainly innervate the LH[20], our findings that chemoactivation of DMH glutamatergic neurons innervated by vmPFCs promoted wakefulness suggest activation of vmPFC-DMH-LH projections for promotion of wakefulness. To vigorously test the vmPFC-DMH-LH circuit as a whole in promoting wakefulness, we conducted a sophisticated experiment instead of a simple photostimulation of vmPFC-DMH-LH terminals. We injected both PRV-Cre and AAV-Camk2-eNpHR3.0-mCherry into bilateral DMHs for a retrograde transport of PRV-Cre back to vmPFC cell bodies and an anterograde transport of inhibitory AAV-Camk2-eNpHR3.0-mCherry to DMH projections in LHs. Four weeks later, AAV-Camk2-DIO-ChR2-

mCherry was injected into bilateral vmPFCs, followed by implantation of a pair of optic fibers vertically above bilateral vmPFCs and another pair of optic fibers above bilateral LHs at 40° oralward angle (Extended Data Fig. 9a). As expected, mice with virus injection confined to bilateral vmPFCs and DMHs (Extended Data Fig. 9b,f,g) kept NREM sleep after 10 Hz photostimulation of vmPFC neurons innervating the DMH and a simultaneous photoinhibition (200 ms, 5 mW, 3 Hz, 10 sec with 10 sec interval) of LH inputs from DMHs, whereas photostimulation alone without photoinhibition in the same mice rapidly switched NREM sleep to wakefulness (Extended Data Fig. 9d,e and Movie S3). Photostimulation during REM sleep did not waken the same mice (Extended Data Fig. 9c). Thus, the LH is the down-stream brain region of the vmPFC-DMH projection for promotion of wakefulness and suppression of NREM sleep.

Inhibition of vmPFC outputs in DMHs suppresses wakefulness and promotes NREM sleep
To access whether vmPFC neurons innervating DMHs are required for physiological sleep-wake behavior, we performed chemoinhibition of vmPFC projections in DMHs. Mice received AAV-Camk2-hM4Di-mCherry (or AAV-Camk2-mCherry as control) injection into bilateral vmPFCs, followed by insertion of 1 pair of cannulae above bilateral DMHs at 40° oralward angle (Fig. 6a). Five weeks later, mice received CNO injection into bilateral DMHs through cannulae at 10:00 pm, a time approximating peak activity in mice. In mice with virus injection confined to bilateral vmPFCs and DMHs (Fig. 6b,c), CNO but not vehicle significantly suppressed wakefulness and promoted NREM sleep without significant effects on REM sleep (Fig. 6d,e). Thus, activation of vmPFC neurons innervating the DMH is required for physiological sleep-wake behavior. Moreover, inhibition of vmPFC projections in DMHs mimicked the effects of cannabinoids on NREM sleep and wakefulness.

While optoactivation of vmPFC-DMH projections switched NREM sleep to wakefulness, we next asked if their optoinhibition could switch wakefulness to NREM sleep. Following AAV-Camk2-eNpHR3.0-mCherry (or AAV-Camk2-mCherry as control) injection into bilateral vmPFCs, a pair of optic fibers were implanted above bilateral DMHs at 40° oralward angle (Fig. 7a). Five weeks later, we applied yellow laser illumination of 200 ms (5 mW, 3 Hz, 10 sec with 10 sec interval) with 20 ms as control. After 200-ms illumination, mice receiving virus injection confined to bilateral vmPFCs (Fig. 7b and Extended Data Fig. 9h) showed approximately 40 sec to NREM sleep (Fig. 7c,d and Extended Data Movie S4). However, after 200-ms illumination to either control mice or mice with virus injection outside unilateral or bilateral vmPFCs, or 20-ms illumination to either control mice or mice with virus injection confined to bilateral vmPFCs, freely moving mice spent approximately 110 sec to NREM sleep for approximately 120 sec (Fig. 7d and Extended Data Fig. 9h). Thus, optoinhibition of vmPFC projections in DMHs switched wakefulness to NREM sleep.

Calcium imaging of vmPFC neurons innervating DMH and PVT

Next, we examined the real-time activity of vmPFC neurons innervating the DMH and PVT across sleep-wake cycle. Calcium activity of the vmPFC was recorded through a photometry fiber implanted above the vmPFC in freely moving mice after injection of the retrograde-tracing AAV2 (rAAV2) expressing the calcium indicator GCaMP6 into the DMH (Fig. 7e) or PVT (Extended Data Fig. 10a). During each imaging session, sleep-wake states were monitored with EEG and EMG recordings. Calcium activity of vmPFC neurons innervating the DMH varied significantly across sleep-wake states, with significant inhibition during NREM sleep and significant activation during wakefulness and REM sleep (Fig. 7f-h). However, calcium activity

of vmPFC neurons innervating the PVT did not show significant changes across sleep-wake states (Extended Data Fig. 10b-d). These results suggest that vmPFC neurons innervating the DMH represent a new class of wake-promoting neurons in the brain.

Chemoactivation of vmPFC neurons innervating DMHs blocks cannabinoid promotion of NREM sleep

While inhibition of DMH glutamatergic but not GABAergic neurons innervated by vmPFC glutamatergic neurons promoted NREM sleep and suppressed wakefulness, cannabinoids, which suppressed DMH glutamatergic but not GABAergic inputs synapsing with DMH glutamatergic but not GABAergic neurons, promoted NREM sleep and suppressed wakefulness. Thus, activation of vmPFC neurons innervating DMHs may block cannabinoid promotion of NREM sleep. To assess this idea, we injected AAV-Camk2-DIO-hM3Dq-mCherry (or AAV-Camk2-DIO-mCherry as control) into bilateral vmPFCs 5 weeks after intra-DMH injection of PRV-Cre (Fig. 8a). In mice receiving AAV-Camk2-DIO-hM3Dq-mCherry, but not AAV-Camk2-DIO-mCherry, within bilateral vmPFCs together with PRV-Cre confined in bilateral DMHs (Fig. 8b and Extended Data Fig. 11), CNO (0.5 mg/kg, i.p.) but not vehicle significantly suppressed NREM sleep and promoted wakefulness without significant effects on REM sleep (Fig. 8c-e). These results replicated our findings shown above that activation of DMH-projecting vmPFC neurons, their terminals or their postsynaptic glutamatergic neurons promoted wakefulness and suppressed NREM sleep without significant effects on REM sleep. Systemic nabilone significantly promoted NREM sleep and suppressed wakefulness, which was blocked by CNO injection (Fig. 8c-e). Our results suggest that cannabinoids promote NREM sleep and suppress wakefulness through inhibition of vmPFC glutamatergic projections in the DMH.

Discussion

The cerebral cortex processes high-order information, but whether the cerebral cortex has wake-promoting cells remains unknown. Our results reveal that activation of vmPFC neurons innervating the DMH is both sufficient and necessary for promotion of wakefulness. Thus, photoactivation of DMH-projecting vmPFC neurons, their terminals or their postsynaptic neurons rapidly and reliably switched NREM sleep to wakefulness, which was blocked by a simultaneous photoinhibition of DMH outputs in LHs. Remarkably, chemoinhibition of vmPFC outputs in DMHs suppressed wakefulness and promoted NREM sleep, suggesting that a basal activation of vmPFC neurons innervating the DMH is required for physiological sleep-wake behavior. Indeed, vmPFC neurons innervating DMHs were active during wakefulness and inactive during NREM sleep. Thus, vmPFC neurons innervating the DMH represent the first identified set of the cerebral cortical neurons for promotion of physiological wakefulness.

In addition to glutamatergic neurons, the DMH also contains a predominant number of GABAergic neurons projecting to the ventrolateral preoptic area (VLPO) of the hypothalamus[20], which plays an important role in modulation of sleep-wake states[20]. A recent study showed that the VLPO received inputs from DMH galanin-expressing GABAergic neurons consisting of NREM-on/REM-off and REM-on/NREM-off neurons without significant involvement in wakefulness[19]. If both NREM-on/REM-off and REM-on/NREM-off neurons projecting to the VLPO are simultaneously activated, the net effect could be insignificant on sleep, which may likely explain our findings that chemoactivation of vmPFC-DMH postsynaptic GABAergic neurons did not significantly affect sleep-wake states.

Dan's group recently hypothesized a new model of an arousal-action circuit for the transition of wake and REM and NREM sleep, with wake-promoting neurons consisting of both action cells being active during wakefulness and arousal cells being active during both wakefulness and REM sleep[11]. Action cells include orexin neurons in the LH and monoaminergic neurons in the brainstem, whereas arousal cells are located in the basal forebrain and PVT[11]. According to this model, vmPFC neurons innervating the DMH belong to arousal cells as they were active during both wakefulness and REM sleep. Although arousal cells are active during both wakefulness and REM sleep, their activation promotes wakefulness without significant effects on REM sleep, because they excite action neurons for motor activation[11]. Interestingly, we found here that photostimulation of vmPFC neurons innervating the DMH led to activation of glutamatergic inputs in the LH, where action orexin cells are located.

When wake-promoting cells in the basal forebrain, LH and brainstem send wake-promoting signals to the mPFC, the mPFC may in turn modulate arousal and wakefulness through its top-down outputs to major wake-promoting neurons in the basal forebrain, LH and brainstem[12,40]. Because the vmPFC exclusively targets GABAergic neurons in both the LC[41] and dorsal raphe nucleus[42], activation of vmPFC neurons likely inhibit noradrenergic neurons in the LC and serotonergic neurons in the raphe nuclei, thus suppressing wakefulness. With sparse labelling approach[34], we found here that wake-promoting vmPFC neurons innervating the DMH did not project to the wake-promoting PVT, LH, tuberomammillary nucleus, basal forebrain, VTA, raphe nuclei, LC and parabrachial nucleus. Therefore, LC- and raphe-projecting vmPFC neurons, activation of which likely suppresses wakefulness, are different from DMH-projecting vmPFC neurons, activation of which promotes wakefulness. It is not clear whether activation of vmPFC neurons innervating the LC and raphe nuclei is required for physiological sleep-wake states.

In sharp contrast to wake-promoting and NREM-suppressing effects produced by activation of vmPFC-DMH projections, a single dose of synthetic cannabinoids significantly promoted NREM sleep and suppressed wakefulness for over 12 hours, which were inhibited by systemic or intra-DMH injection of CB_1R antagonist AM281 and blocked by chemoactivation of vmPFC neurons innervating DMHs. Surprisingly, cannabinoids selectively activated CB_1R at DMH glutamatergic but not GABAergic inputs synapsing with DMH glutamatergic but not GABAergic neurons, thus inhibiting DMH glutamatergic but not GABAergic neurons. These results further support the idea that activation of vmPFC neurons innervating DMH neurons is required for physiological sleep-wake behavior. NREM sleep is important for restoration of body physiology especially brain function[43] and memory consolidation[44]. Therefore, our findings that nabilone significantly promoted the quality of NREM sleep, i.e. increased bout duration of NREM sleep, indicate therapeutic application of nabilone for the treatment of sleep disorders, which affect approximately 1/4 of human population[1]. Notably, clinical studies indicate that nabilone was not associated with the development of tolerance and had little evidence for abuse or addiction due to less euphoric effects[45].

Both nabilone and HU210 prominently suppressed REM sleep, which was not affected by systemic or intra-DMH administration of CB_1R antagonist AM281 or by chemoactivation of vmPFC neurons innervating the DMH. Interestingly, neither activation nor suppression of vmPFC-DMH projections significantly affected REM sleep.

In conclusion, vmPFC neurons innervating the DMH represent the first identified set of cerebral cortical cells for promotion of physiological wakefulness and suppression of NREM sleep without significant involvement in REM sleep (Fig. 8f). In contrast, synthetic cannabinoids produce profound promotion of NREM sleep and suppression of wakefulness through activation

19

of CB_1R at vmPFC glutamatergic inputs synapsing with DMH glutamatergic neurons, thus inhibiting DMH glutamatergic neurons (Fig. 8g).

Methods

Animals

We used adult (over 2 months old) male CD1 mice, vGlut2-iCreERT2 mutant mice carrying iCreERT2 in brain glutamatergic neurons containing vGlut2, and Dlxa-Cre mice carrying Cre in forebrain GABAergic neurons, which were used in our recent studies[36,39]. Mice were housed under standard housing conditions (7:00 am lights-on/7:00 pm lights off, 22±2°C, food and water *ad libitum*). Animal use and care was under the guidelines established by Qingdao University of China, University of Ottawa Institute of Mental Health Research of Canada, and Fourth Military Medical University of China. All the raw data used in this study were recorded on experimental book or tapes or collected in computer.

Sleep-wake recording and analysis

Under anesthesia with isoflurane (4% for induction, 1.5% for maintenance), an adult mouse was placed in a stereotaxic apparatus. A longitudinal incision of 1 cm in length was made in the midline and through the scalp to expose the skull for implantation of the EEG/EMG headmount (8402, Pinnacle Technology Inc., USA) onto the mouse skull (AP 3 mm) with stainless steel screws serving as EEG electrodes across the cortex. Dental acrylic was applied to secure the headmount in place. EMG probes were inserted into the cervical portion of the trapezoid muscles. Metacam (0.2 mg/kg, s.c.) was injected once per day for 3 days after surgery. After surgery, mice were allowed to recover undisturbed for at least 1 week before they were briefly anesthetized

with isoflurane (4% induction, 1.5% maintenance) and the headstage pre-amplifier (8406, Pinnacle Technology Inc., USA) was attached to a connector of the mouse EEG headmount. Mice were then returned to their Plexiglas recording cages (25.4 cm in diameter and 20.3 cm in height) and were left undisturbed until they were habituated to being chronically tethered and exhibited a regular sleep-wake cycle; typically 5 to 7 days. Then, baseline EEG/EMG was recorded for 24 h starting at 7:00 am. Using Sirenia® Sleep Pro (Pinnacle Technology Inc., USA), polysomnographs were digitally filtered and analyzed by scoring 4-sec epochs (optogenetic and chemogenetic) or 2-sec (probability analysis), and corrected manually according to standard criteria: (1) wakefulness was defined as theta waves (4-8 Hz), alpha waves (8-14 Hz), beta waves (14-30 Hz) and gamma waves (30-100 Hz) on EEG and elevated EMG activity with phasic bursts; (2) NREM sleep was defined as synchronized, high amplitude Delta waves (1-4 Hz) on EEG activity and lower EMG activity compared with wakefulness with no phasic bursts; and (3) REM sleep was defined as containing theta waves (4-8 Hz) on EEG with nearly no EMG activity.

We analyzed EEG traces with custom written MATLAB scripts and functions (MathWorks). EEG traces were band-pass filtered in the forward and reverse direction to eliminate phase distortions. Spectral analysis (spectrogram plotting) was performed using a multi-taper fast Fourier transform (FFT, padding factor =1) on each 40-50s data segments taken before and after optical stimulation (Chronux package, window = 4 s, step = 0.5 s, tapers [2 3]). Power spectra were calculated in a linear scale to achieve the power distribution in the frequency band of interest (0-20 Hz). EEG power value was extracted from the power spectrum (band power: total power over 0.5-20 Hz). Power spectral density was calculated by the Fourier transform of the

autocorrelation. EEG peak frequency was extracted from the power spectral density. EEG was sampled at 400 Hz.

We also analyzed EEG brain waves before, during and after photostimulation in mice receiving photostimulation of postsynaptic DMH neurons of vmPFC-DMH projections. The absolute EEG waves were analyzed off-line with Lab Chart 7 software. The duration of each data segment is 50s including Base (20s), Light (10s) and Post (20s). The absolute waves within 6 frequency bands were calculated: δ (delta, 1–4 Hz); θ (theta, 4–8 Hz); α (alpha, 8–12 Hz); β (beta, 12–30 Hz); γ (gamma, 30–100 Hz); and total power (0–100 Hz).

Cannabinoid treatment

Under anesthesia with isoflurane, the EEG/EMG headmount was placed onto the mouse skull and secured, after which mice for future intra-DMH injection received placement of double cannulae (Plastics One, Canada) above bilateral DMHs (AP –1.67, ML ±0.4, DV –4.3 mm) and then secured. Three weeks later, we injected nabilone (0.2, 1.0, 5.0 mg/kg; Tocris Bioscience, Ellisville, USA; dissolved in 5% DMSO and 5% Tween-80 in physiological saline), HU210 (10, 20, 50 μg/kg, i.p.; Tocris Bioscience, Ellisville, USA; dissolved in 5% DMSO and 5% Tween-80 in physiological saline) or AM281 (2 mg/kg, i.p.; 50 ng/0.2 μl/side, intra-DMH; Tocris Bioscience, Ellisville, USA; dissolved in 5% DMSO and 5% Tween-80 in physiological saline) at 7:50 AM (i.p. injection of nabilone, HU210 or AM281 alone) with or without i.p. or intra-DMH pretreatment of AM281 or vehicle at 7:30 AM. Using precision syringe pumps (Harvard Apparatus, USA), we conducted intra-DMH microinjection of AM281 through a pair of previously implanted cannulae (1 mm extended out of the guide cannula) at a rate of 0.1 μl/min

for 2 min. Localization of AM281 injection sites was done by measuring the distance of 1 mm below the cannulae tract tip.

Viral preparation

PRV-Cre was produced as shown in our recent study[36]. The AAV-Camk2-DIO-ChR2-mCherry, AAV-Camk2-DIO-mCherry, AAV-Camk2-ChR2-mCherry, AAV-Camk2-mCherry, AAV-Camk2-hm3Dq-mCherry, AAV-EF-A-DIO-EGFP, AAV-EGFP and AAV-Camk2-DIO-eNpHR3.0-mCherry were purchased from the Neurophotonics platform at University of Laval, Quebec, Canada. The rAAV2-retro-Syn-GCaMP6, pAAV-hSyn-EGFP-2A-Cre, pAAV-EF1a-DIO-ChR2-mCherry, pAAV-EF1a-DIO-mCherry, pAAV-hSyn-DIO-EGFP-T2A-NLS-Flipo, pAAV-EF1a-fDIO-hM3Dq-mCherry, pAAV-EF1a-fDIO-hM4Di-mCherry, pAAV-EF1a-fDIO-mCherry, pAAV-EF1a-fDIO-eNpHR3.0-mCherry, pAAV-SYN-MCS-mCherry-3FLAG, pAAV-SYN-MCS-EGFP-3FLAG, rAAV2-Camk2-mCherry-2A-Cre, pAAV-TRE-DIO-FLPo and pAAV-TRE-fDIO-GFP-IRES-Tta were purchased from OBiO technology (He Yuan) Corp. Shanghai, China. Aliquots of viral vectors were stored at -80°C before experiments. Animals received viral injections (0.1 μl, titer 10^{12} particles per ml) under anesthesia with isoflurane (4% for induction, 1.5% for maintenance).

Electrophysiology analysis

After decapitation, the mouse brain was removed and coronal brain vibrosections (300 μm) were cut and maintained in the artificial cerebral spinal fluid (ACSF) (in mM: 125 NaCl, 25 $NaHCO_3$, 1.25 KCl, 1.25 KH_2PO_4, 1.5 $MgCl_2$, 1 $CaCl_2$, and 16 glucose) saturated with 95% O_2-5% CO_2. The patch pipettes contained an intracellular solution (in mM: 120 K gluconate, 20 KCl, 10

HEPES, 10 phosphocreatine Na salt, 2 ATP Na salt, 0.4 GTP Na salt, 2 MgCl$_2$, pH 7.35). To identify the electrical fingerprints of mCherry expressing vmPFC or DMH neurons, cells were visually identified under the florescent microscope and current clamped at -70 mV, and then a negative current step (-20 pA, 1 s) was delivered and followed by a series of 2-s positive current steps from -20 to +200 pA. The distinct firing properties of the DMH neurons were collected and distinguished. The photo-current/voltage responses of the virus expressing vmPFC cells to a variety of optical stimulation frequency (1-50Hz) were collected afterwards. The firing property of DMH neurons were recorded before and after bath application of CNO.

To record EPSCs and IPSCs, ASCF was supplemented with 50 μM D-APV and 10 μM BMI (EPSCs) or 10 μM CNQX (IPSCs). To record postsynaptic currents (PSCs), neurons were whole-cell voltage clamped at −70 mV with a Multiclamp 700B amplifier (Molecular Devices). To evoke PSCs, a stable whole-cell recording configuration was established on the DMH cell. Then, a second stimulation glass electrode (2-6 MΩ) filled with 2M NaCl was lowered into the slice with 100 μm away from the recording site. PSCs were collected by voltage clamp recordings using a stimulus pulse of a single square wave (stimulation intensity: 100 μsec, 50–200 μA). To evoke DSI/DSE at 4-s intervals, cells were depolarized from -70 to 0 mV for 5 s. Nabilone or HU210 dissolved in DMSO was directly added into the perfusion ACSF solution to achieve the final concentration 1 mg/100 ml. The data were acquired with pCLAMP 10.4 (Molecular Devices) at a sampling rate of 5–10 kHz, measured and plotted with pCLAMP 10.0 and GraphPad prism 6.0.

To characterize DSE in DMH GABAergic neurons, we directly prepared hypothalamic slices from the GABA transgenic mice, followed by identification and recording of the fluorescent positive DMH neurons. To examine electrophysiology of DMH glutamatergic neurons, we

injected AAV-mCherry (3.3 X 10^{12} genome copies per ml), at a rate of 0.15 μl/min for 2 min, into the DMH of the young vGlut2-iCreERT2 mutant mice. After surgery, the mice received tamoxifen injection (1 mg/mouse/day) for 8 days. Two weeks after surgery, mice were killed for preparation of hypothalamic slices as described above. The mCherry positive DMH neurons were identified and recorded to characterize DSE. After acquisition of stable recordings for 5–7 min, ACSF solution containing HU210 or nabilone was perfused. DSE was recorded, measured and plotted with pCLAMP 10.0 and GraphPad prism 6.0.

Identification of DMH glutamatergic and GABAergic neurons

To identify DMH glutamatergic neurons under fluorescent microscopy, we injected AAV-DION-mCherry into the DMH of our vGlut2-iCreERT2 mutant mice[36]. The fluorescence labeled and unlabeled neurons in the DMH showed LTS(-) and LTS(+), respectively, signifying that DMH LTS(-) neurons but not LTS(+) neurons are glutamatergic neurons. The GABA transgenic mice selectively expressing enhanced green fluorescent protein (eGFP) in GAD67-synthesizing neurons were provided by Dr. Yanagawa. The eGFP-labeled and unlabeled neurons in the DMH showed LTS(+) and LTS(-), respectively, signifying that DMH LTS(+) neurons but not LTS(-) neurons are GABAergic neurons.

Neuroanatomical tract-tracing experiments

Adult male CD1 mice were anesthetized with isoflurane (4% induction, 1.5% maintenance) and placed on a stereotaxic apparatus. Ophthalmic ointment was smeared to the eyes to prevent drying. After shaving the hair and cleaning the incision site with medical alcohol and iodine, the scalp was incised to expose the skull and the connective tissue was gently removed from the

skull surface with cotton tips. Small craniotomy holes (1 mm diameter) were drilled with the help of microscope for virus injection (0.1 μl, in 10 min; Obio Technology Co. Ltd., China) using microliter syringe (Hamilton 7001KH, Switzerland). Animals received pAAV-SYN-MCS-mCherry-3FLAG injection into the DMH (AP −1.67, ML +0.4, DV −5.3 mm) with or without subsequent injection of pAAV-SYN-MCS-EGFP-3FLAG into the PVT (AP −1.40, ML 0, DV −3 mm). After injection, the syringe was left in place for an additional 10 min before closing the skin with surgical sutures. Four weeks after surgery, mice were anesthetized with 5% chloral hydrate (8 mg/kg, i.p.) and perfused transcardially with normal saline, followed by 100 ml ice-cold 4% paraformaldehyde in PBS. Brains were carefully removed from the skull and postfixed in 4% paraformaldehyde for 12 hours, then dehydrated with 30% sucrose at 4°C overnight. With a freezing microtome (CM 3050S, Leica), brains were cut into 40-μm coronal sections, which were then mounted onto glass slides. Histological images were acquired with an upright fluorescent microscope (Nikon).

Sparse labeling and brain clarity experiments

Under anesthesia with isoflurane (4% for induction, 1.5% for maintenance), adult CD1 mice were injected with 0.1 μl of rAAV2-Camk2-mCherry-2A-Cre into the DMH (AP –1.67, ML –0.4, DV –5.3 mm) and 0.1 μl of both pAAV-TRE-DIO-FLPo and pAAV-TRE-fDIO-GFP-IRES-Tta into the ipsilateral vmPFC (AP +1.9, ML –0.3, DV –2.7 mm) at a speed of 40 nl/min. Five weeks later, mice brains were dissected and post-fixed in 4% paraformaldehyde for 24 h at 4 °C. The brains were rinsed in 0.01 M PBS three times. We then use the X-Clarity tissue clearing system (C30001, Logos Biosystems, South Korea) to clear brains[35]. Briefly, the whole mouse brain was soaked in a mixture of 5 ml Hydrogel Solution and 12.5 mg Polymerization Initiator (C1310X,

Logos Biosystems, South Korea) at 4°C for 24 h, followed by centrifuge with the polymerization system (C20001, Logos Biosystems, South Korea) at 37 °C and -90 kPa pressure for 3 h. After polymerization, the brain was washed with 1×PBS at room temperature 3×5 min. The whole brain was cleared in a container at 37 °C and RPM 100 for 8 h,. After wash for 6×30 min with 0.01 M PBS, the brain was placed into 5 ml of Mounting Solution solution (C13101, Logos Biosystems, South Korea) for 2 h and then transfered into 20 ml of Mounting Solution at 37° in the dark for overnight. With the Light Sheet Microscope (Light-sheet Z.1, Carl Zeiss, Germany.), the cleared brains were imaged in a sagittal plane in GFP channels. The image preprocessing was performed using Imaris (version 9.5, Oxford Instruments, UK).

Optogenetic experiments

CD1 mice were injected with the following viruses in different experiments: (1) PRV-Cre (together with 10:1 of AAV-EF-A-DIO-mCherry for locatization of PRV-Cre injection sites) into the bilateral DMHs (AP –1.67, ML ±0.4, DV –5.3 mm), followed 5 weeks later by AAV-Camk2-DIO-ChR2-mCherry (or AAV-Camk2-DIO-mCherry as control) into bilateral vmPFCs (AP +1.9, ML ±0.3, DV –2.7 mm); (2) AAV-Camk2-ChR2-mCherry (or AAV-Camk2-mCherry as control) into bilateral vmPFCs; (3) pAAV-hSyn-EGFP-2A-Cre into bilateral vmPFCs, followed 5 weeks later by pAAV-EF1a-DIO-ChR2-mCherry (or pAAV-EF1a-DIO-mCherry as control) into bilateral DMHs; (4) AAV-Camk2-eNpHR3.0-mCherry (or pAAV-Camk2-mCherry as control) into bilateral vmPFCs; and (5) both PRV-Cre and AAV-Camk2-eNpHR3.0-mCherry into bilateral DMHs, followed 4 weeks later by AAV-Camk2-DIO-ChR2-mCherry into bilateral vmPFCs; (6) AAV-Camk2-ChR2-mCherry (or AAV-Camk2-mCherry as control) into the PVT (AP −1.40, ML 0, DV −3 mm). Dlxa-Cre mice received injection of the

following viruses: pAAV-hSyn-DIO-EGFP-T2A-NLS-Flipo into bilateral vmPFCs, followed 1 week later by pAAV-EF1a-fDIO-ChR2-mCherry (or pAAV-EF1a-fDIO-mCherry as control) injection into bilateral DMHs.

At the end of the last surgery, the EEG/EMG headmount was placed onto the mouse skull and secured, after which an optical fiber housing unit or double cannulae (Plastics One, Canada) was placed above the skull with the fiber or cannula insertion vertically above bilateral vmPFCs (AP 1.9, ML ±0.3, DV –2.7mm) or toward DMH (AP –3.13, ML ±0.4, DV –6.55 mm, with 40° oralward angle), LH (AP –3.13, ML ±1.05, DV −6.53 mm, with 40° oralward angle) or PVT (AP +1.55, ML 0.55, DV −4.3 mm, with 45° caudalward angle and 10° towards the midline), and then secured. Four to six weeks after surgery, an optic fiber patch cord assembled with a standard kit (Plastic one, Canada) was connected to the optic fiber cannulae. Blue light (450 nm wavelength) or yellow (594 nm wavelength) light (Thinker Tech Nanjing BioScience Inc., Nanjing, China) was delivered to the specific brain regions through a TTL controlled laser (Thinker Tech Nanjing BioScience Inc., Nanjing, China) with adjustable output intensity via the optic fiber patch cord-optic fiber implant system (Plastic One, Canada). In brain slices, we applied blue laser light stimulation of 1, 10, 20 or 50 Hz (5 mW, 10 ms each pulse, 10 sec total). For blue light photostimulation in freely moving animals, each mouse received at least 3 trains of 1-Hz and 10-Hz stimuli for 10 seconds with 40-60 min interval between each train. The interval was not fixed due to the variability of each sleep bout length. The same photostimulation protocol was used throughout all experiments in this study. For yellow light photosuppression in freely moving animals, we applied yellow laser illumination of 200 ms (5 mW, 3 Hz, 10 sec with 10 sec interval) with 20 ms as control. For each AAV-ChR2/AAV-eNpHR3.0 transduced mouse, the minimum amount of light estimated to be present at the tip of the optic fiber implant required

to produce maximal effects on wakening effects during NREM/REM sleep was determined in advance in order to minimize unwanted side-effects including light-induced tissue damage as well as excessive disturbance of animals. The estimation was based on pre-surgery testing of transmittance of light through the optic fiber patch cord (Thorlabs, USA) and optic fiber implant. The amount of light determined using these criteria were below 25 mW. The amount of light that each control AAV-mcherry injected mouse received during all optical experiments was matched with an AAV-ChR2/AAV-eNpHR3.0 transduced mouse.

Chemogenetic study

For chemogenetic study on CD1 mice, PRV-Cre (together with 10:1 of AAV-EF-A-DIO-mCherry for locatization of PRV-Cre injection sites) into the bilateral DMHs (AP –1.67, ML ±0.4, DV –5.3 mm). Five weeks later, mice received an injection of AAV-Camk2-hM3Dq-mCherry (or AAV-Camk2-mCherry as control) into bilateral vmPFCs, followed by a placement of the EEG/EMG headmount onto the mouse skull and secured. Four weeks later mice received an injection of CNO (0.5 mg/kg, i.p.; Cayman Chemical, USA) or vehicle with or without nabilone injection (1 mg/kg, i.p.). Other CD1 mice received an injection of AAV-Camk2-hM4Di-mCherry (or AAV-Camk2-mCherry as control) into bilateral vmPFCs, and then a pair of cannulae were placed 1 mm above bilateral DMHs (AP –3.13, ML ±0.4, DV –6.1 mm, with 40° oralward angle) for future CNO injection, followed by a placement of the EEG/EMG headmount onto the mouse skull and secured. For chemogenetic study on vGlut2-icreERT2 mice, pAAV-hSyn-DIO-EGFP-T2A-NLS-Flipo was injected bilaterally into the vmPFC (AP 1.9, ML ±0.3, DV –2.7 mm). Five weeks later, mice received an injection of pAAV-EF1a-fDIO-hM3Dq-mCherry or control virus (pAAV-EF1a-fDIO-mCherry) into bilateral DMHs. Next, the

EEG/EMG headmount was placed onto the mouse skull and secured. For chemogenetic study on Dlxa-Cre mice, pAAV-hSyn-DIO-EGFP-T2A-NLS-Flipo was injected into bilateral vmPFCs, followed 4 weeks later by pAAV-EF1a-fDIO-hM3Dq-mCherry or control virus (pAAV-EF1a-fDIO-mCherry) injection into bilateral DMHs. Next, the EEG/EMG headmount was placed onto the mouse skull and secured. After surgery, the vGlut2-icreERT2 mice also received tamoxifen injection (1 mg/mouse/day, dissolved in corn oil) for 8 days. Four to six weeks after surgery, all mice received baseline EEG/EMG recording for 24 hours before an i.p. injection of CNO (0.5 mg/kg, i.p.) or vehicle at 10:00 AM or a bilateral intra-DMH injection of CNO (10 μM/0.2 μl/side) or vehicle. We conducted intra-DMH microinjection of CNO by extending 1 mm out of the implanted cannulae at a rate of 0.1 μl/min for 2 min. Localization of CNO injection sites was done by measuring the distance of 1 mm below the cannulae tract tip.

Confirmation of virus injection sites

After experiments, mice were anesthetized with 5% chloral hydrate (8 mg/kg, i.p.) and perfused transcardially with normal saline, followed by 100 ml ice-cold 4% paraformaldehyde in PBS. Brains were carefully removed from the skull and postfixed in 4% paraformaldehyde for 12 hours, then dehydrated with 30% sucrose at 4°C overnight. With a freezing microtome (CM 3050S, Leica), brains were cut into 40-μm frontal sections, which were then mounted onto glass slides. Histological images were acquired with an upright fluorescent microscope (Nikon). Finally, we identified and recorded locations of central points of virus injection sites within (black circles) bilateral and outside (white circles) unilateral or bilateral or within unilateral vmPFCs or DMHs. For intra-DMH injection of AM281 or CNO, the injection sites were 1 mm below the tips of bilateral cannulae. For each experiment, we routinely conducted numerous

mice until 5 mice receiving target virus and 5 mice receiving control virus or 6 mice receiving intra-DMH injection of AM281 showed injection sites within bilateral vmPFCs and/or DMHs.

Fiber photometry

Under anesthesia with isoflurane (4% for induction, 1.5% for maintenance), adult C57/BL6 mice received rAAV2-retro-Syn-GCaMP6 injection into the DMH (AP –1.67, ML –0.4, DV –5.3 mm) or PVT (AP −1.40, ML 0, DV −3 mm) at a speed of 40 nl/min. After viral injection, a photometry fiber was implanted ipsilaterally 100 μm above the vmPFC area (AP +1.9, ML –0.3, DV –2.7 mm), after which the EEG/EMG headmount was placed onto the mouse skull and secured. Four weeks later, we cellected photometry signal data after the signal became stable. For each test, the photometry signal F was converted to Δ F/F as following formula by Matlab. At the same time, we recorded EEG and EMG for 1-2 sessions, each with 1-4h duration. To analyze sleep-wake states, we selected all the sessions in which mice had all three states, i.e. NREM, REM and wakefulness, followed by calculation of Δ F/F photometry ratios during contiguous three sleep-wake states. After collecting data, mice were anesthetized with 5% chloral hydrate (8 mg/kg, i.p.) and perfused transcardially with normal saline and 4% paraformaldehyde in PBS. Brains were dehydrated with 30% sucrose at 4°C overnight and cut with a freezing microtome for localization of both the DMH or PVT injection site and vmPFC fiber site.

$$F_0 = \overline{V_{basal}} \qquad \frac{\Delta F}{F_0} = \frac{V_{signal} - F_0}{F_0 - V_{offset}}$$

$\overline{V_{basal}}$: average value of V_{basal} in reference time

Statistical analysis

Results were reported as mean ± SEM. Statistical analysis of the data was performed using a Student t test, one-way ANOVA, two-way ANOVA, two-way ANOVA for repeated measures or RM two-way ANOVA, followed by Bonferroni *post-hoc* test. Statistical significance was set at $p<0.05$ (*), $p<0.01$(**).

Author contributions

X.X., H.Z., H.X. and N.G. conducted major fiber photometry, optogenetic, chemogenetic and neuroanatomical experiments and designed the experiments with H.D. and X.Z. X.L., R.X., Y.W., L.T., Q.Z., J.X., X.X., H.Z., N.G. and H.D. participated in conducting some experiments and analysis of fiber photometry, optogenetic and chemogenetic data. X.Z. conceived the project and wrote the manuscript with the help of H.D., N.G., L.Z., Z.H. and J.H.

References

1   Collins, F. S. National Institutes of Health Sleep Disorders Research Plan,
        http://www.nhlbi.nih.gov/files/docs/resources/sleep/201101011NationalSleepDisordersRe
        searchPlanDHHSPublication11-7820.pdf (National Institutes of Health, June 1, 2011).

2   Weber, F. & Dan, Y. Circuit-based interrogation of sleep control. *Nature* **538**, 51–59
        (2016).

3   Buonamici, M., Young, G. A. & Khazan, N. Effects of acute delta 9-THC administration
        on EEG and EEG power spectra in the rat. *Neuropharmacol.* **21**, 825–829 (1982).

4   Goonawardena, A. V. et al. A Pilot study into the effects of the CB1 cannabinoid receptor
        agonist WIN55,212-2 or the antagonist/inverse agonist AM251 on sleep in rats. *Sleep
        Disord.* **2011**, 178469 (2011).

5   Gates, P., Albertella, L. & Copeland, J. Cannabis withdrawal and sleep: A systematic
        review of human studies. *Subst. Abus.*, 1–15 (2015).

6   Barratt, E. S., Beaver, W. & White, R. The effects of marijuana on human sleep patterns.
        Biol. Psychiatry **8**, 47–54 (1974).

7   Whiting, P. F. et al. Cannabinoids for medical use: a systematic review and meta-
        analysis. *JAMA.* **313**, 2456–2473 (2015).

8   Ware, M. A., Fitzcharles, M. A., Joseph, L. & Shir, Y. The effects of nabilone on sleep in
        fibromyalgia: results of a randomized controlled trial. *Anesth. Analg.* **110**, 604–610
        (2010).

9   Jetly, R., Heber, A., Fraser, G. & Boisvert, D. The efficacy of nabilone, a synthetic
        cannabinoid, in the treatment of PTSD-associated nightmares: A preliminary randomized,

double-blind, placebo-controlled cross-over design study. *Psychoneuroendocrinol.* **51**, 585–588 (2015).

10   Murillo-Rodríguez, E., Aguilar-Turton, L., Mijangos-Moreno, S., Sarro-Ramírez, A. & Arias-Carrión, Ó. Chapter 29, Phytocannabinoids as Novel Therapeutic Agents for Sleep Disorders. *Handbook of Cannabis 1st edn* (ed Pertwee, R.), 538–546 (Oxford Univ. Press, 2014).

11   Liu, D. & Dan, Y. A motor theory of sleep-wake control: arousal-action circuit. *Annu. Rev. Neurosci.* **42**, 27–46 (2019).

12   Saper, C. B. & Fuller, P. M. Wake-sleep circuitry: an overview. *Curr. Opin. Neurobiol.* **44**, 186–192 (2017).

13   Scammell, T. E., Arrigoni, E. & Lipton, J.O. Neural circuitry of wakefulness and sleep. *Neuron* **93**, 747–765 (2017).

14   Economo, C. V. Sleep as a problem of localization. *J. Nerv. Ment. Dis.* **71**, 249–259 (1930).

15   Lorincz, M. L. & Adamantidis, A. R. Monoaminergic control of brain states and sensory processing: existing knowledge and recent insights obtained with optogenetics. *Prog. Neurobiol.* **151**, 237–253 (2017).

16   Tyree, S. M. & de Lecea, L. Optogenetic investigation of arousal circuits. *Int. J. Mol. Sci.* **18** (2017).

17   Asghari-Roodsari, A. et al. Tocolytic effect of delta9-tetrahydrocannabinol in mice model of lipopolysaccharide-induced preterm delivery: role of nitric oxide. *Reprod. Sci.* **17**, 391–400 (2010).

18   Lin, Q. S. et al. Hippocampal endocannabinoids play an important role in induction of long-term potentiation and regulation of contextual fear memory formation. *Brain Res. Bull.* **86**, 139–145 (Oxford Press, 2011).

19   Chen, K.S. et al. A hypothalamic switch for REM and non-REM sleep. *Neuron* **97**, 1168–1176 e1164 (2018).

20   Chou, T. C. et al. Critical role of dorsomedial hypothalamic nucleus in a wide range of behavioral circadian rhythms. *J. Neurosci.* **23**, 10691–10702 (2003).

21   Fukushi, I., Yokota, S. & Okada, Y. The role of the hypothalamus in modulation of respiration. *Respir. Physiol. Neurobiol.* **265**, 172–179 (2019).

22   Horiuchi, J., McDowall, L. M. & Dampney, R. A. Differential control of cardiac and sympathetic vasomotor activity from the dorsomedial hypothalamus. *Clin. Exp. Pharmacol. Physiol.* **33**, 1265–1268 (2006).

23   Thompson, R. H. & Swanson, L. W. Organization of inputs to the dorsomedial nucleus of the hypothalamus: a reexamination with Fluorogold and PHAL in the rat. *Brain Res. Rev.* **27**, 89–118 (1998).

24   Chevaleyre, V., Takahashi, K. A. & Castillo, P. E. Endocannabinoid-mediated synaptic plasticity in the CNS. *Annu. Rev. Neurosci.* **29**, 37–76 (2006).

25   Katona, I. & Freund, T. F. Multiple functions of endocannabinoid signaling in the brain. *Annu. Rev. Neurosci.* **35**, 529–558 (2012).

26   Crosby, K. M., Inoue, W., Pittman, Q. J. & Bains, J. S. Endocannabinoids gate state-dependent plasticity of synaptic inhibition in feeding circuits. *Neuron* **71**, 529–541 (2011).

27   Krone, L. et al. Top-down control of arousal and sleep: fundamentals and clinical implications. *Sleep Med. Rev.* **31**, 17–24 (2017).

28   Riga, D. et al. Optogenetic dissection of medial prefrontal cortex circuitry. *Front. Syst. Neurosci.* **8**, 230 (2014).

29   Bienkowski, M.S. et al. Integration of gene expression and brain-wide connectivity reveals the multiscale organization of mouse hippocampal networks. *Nat. Neurosci.* **21**, 1628–1643 (2018).

30   Wood, M. et al. Infralimbic prefrontal cortex structural and functional connectivity with the limbic forebrain: a combined viral genetic and optogenetic analysis. *Brain Struct. Funct.* **224**, 73–97 (2019).

31   Zingg, B. et al. Neural networks of the mouse neocortex. *Cell* **156**, 1096–1111 (2014).

32   Schneider, B. & Koenigs, M. Human lesion studies of ventromedial prefrontal cortex. *Neuropsychologia* **107**, 84–93 (2017).

33   Myers, B., Dolgas, C. M., Kasckow, J., Cullinan, W. E. & Herman, J. P. Central stress-integrative circuits: forebrain glutamatergic and GABAergic projections to the dorsomedial hypothalamus, medial preoptic area, and bed nucleus of the stria terminalis. *Brain Struct. Funct.* **219**, 1287–1303 (2014).

34   Lin, R. et al. Cell-type-specific and projection-specific brain-wide reconstruction of single neurons. *Nat. Methods* **15**, 1033–1036 (2018).

35   Chung, K. et al. Structural and molecular interrogation of intact biological systems. *Nature* **497**, 332–337 (2013).

36   Zhong, H. et al. Endocannabinoid signaling in hypothalamic circuits regulates arousal from general anesthesia in mice. *J. Clin. Invest.* **127**, 2295–2309 (2017).

37   Zingg, B. et al. AAV-mediated anterograde transsynaptic tagging: mapping corticocollicular input-defined neural pathways for defense behaviors. *Neuron* **93**, 33–47 (2017).

38.   Ren, S. et al. The paraventricular thalamus is a critical thalamic area for wakefulness. *Science* **362**, 429–434 (2018).

39   Han, J. et al. Acute cannabinoids impair working memory through astroglial CB1 receptor modulation of hippocampal LTD. *Cell* **148**, 1039–1050 (2012).

40   Aston-Jones, G. & Cohen, J. D. Adaptive gain and the role of the locus coeruleus-norepinephrine system in optimal performance. *J. Comp. Neurol.* **493**, 99–110 (2005).

41   Breton-Provencher, V. & Sur, M. Active control of arousal by a locus coeruleus GABAergic circuit. *Nat. Neurosci.* **22**, 218–228 (2019).

42   Challis, C., Beck, S. G. & Berton, O. Optogenetic modulation of descending prefrontocortical inputs to the dorsal raphe bidirectionally bias socioaffective choices after social defeat. *Front. Behav. Neurosci.* **8**, 43 (2014).

43   Hobson, J. A. Sleep is of the brain, by the brain and for the brain. *Nature* **437**, 1254–1256 (2005).

44   Born, R. B. About sleep's role in memory. *J. Physiol. Rev.* **93**, 681–766 (2013).

45   Ware, M.A. & St Arnaud-Trempe, E. The abuse potential of the synthetic cannabinoid nabilone. *Addiction* **105**, 494–503 (2010).
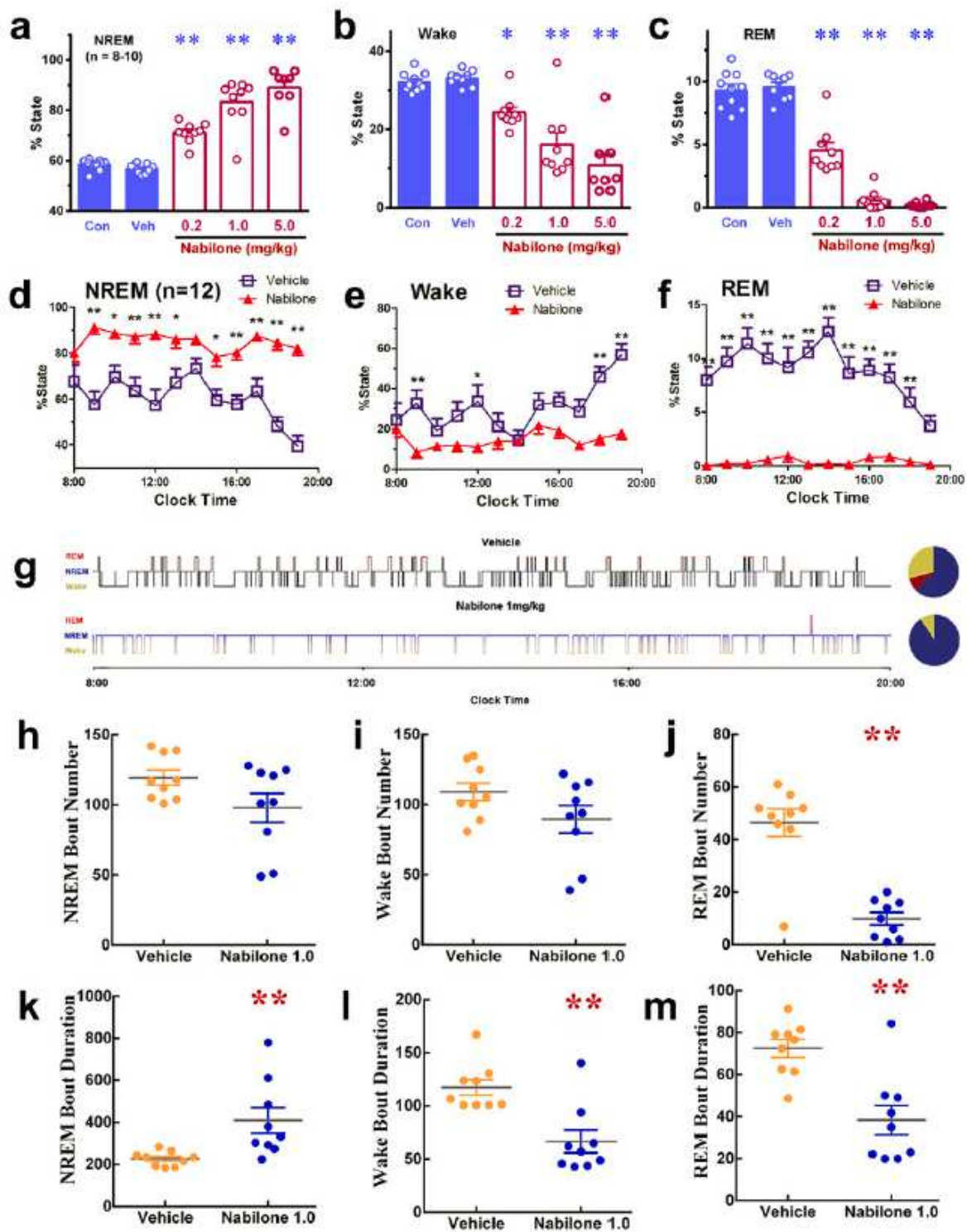
Figures

Figure 1

Nabilone modulation of sleep-wake behavior. a-c, Relative to control mice (Con), nabilone but not vehicle (Veh) dose dependently promotes NREM sleep (a) and suppresses wakefulness (b) and REM sleep (c). d-f, Nabilone (1 mg/kg, i.p.) promotes NREM sleep and suppresses wakefulness and REM sleep for over 12

h . g, Representative 3-hour hypnogram and pie charts before and after a nabilone injection (1 mg/kg, i.p.) . h-j, Bout number of sleep states during light-on period. k-m, Bout length of sleep states during light-on period. Data are means+- SEMs; n = number of mice.* p<0.05 and** p<0.01 vs. control, Bonferronipost-hoc test after on -way ANOVA (a: F4,40 = 53.62, p<0.0 l; b: F4,40 = 26.07, p<0.01; c: F4,40 = 120.6,p<0.0l) or after two-way A.NOVA for repeated measures (d: Fi,176= 1 42.9, p<O. 01; e: F1 ,li6= 61.38,p<0.0l; f F1,1;6 = 87.4 7,p<0.0l). ** p<0.01 vs. vehicle, Student t-test (h-m).

Figure 2

Cannabinoids target glutamatergic inputs onto DMH glutamatergic but not GABAergic neurons. a,b, Plots of normalized IPSC show tha t nabilone does not significantly affect DSI ofDMH LTS(-) (a) and LTS(+) neurons (b). Representative IPSC traces are superimposed on the top of each plot. c-f, Plots of normalized EPSC amplitude show that nabilone (c-f) or HU210 (f) significantly inhibits DSE of DMH LTS(-) neurons (c) and DMH glutamatergic neurons (f) without significant effects on DSE of DMHL TS(+) neurons (d) and DMH GABAergic neurons (e). Representative EPSC traces are superimposed on the top of each plot. g,b, Representative traces show that bath application of nabilone onto hypothalamic slices significantly reduces firing rates of DMH LTS(-) but not LTS(+) neurons. i, Summary graphs show means +- SEMs; n = numbers of mice in each group.** p<0.0 1 vs. control or baseline, Student l-test. C, control; N, nabilone; B, baseline.
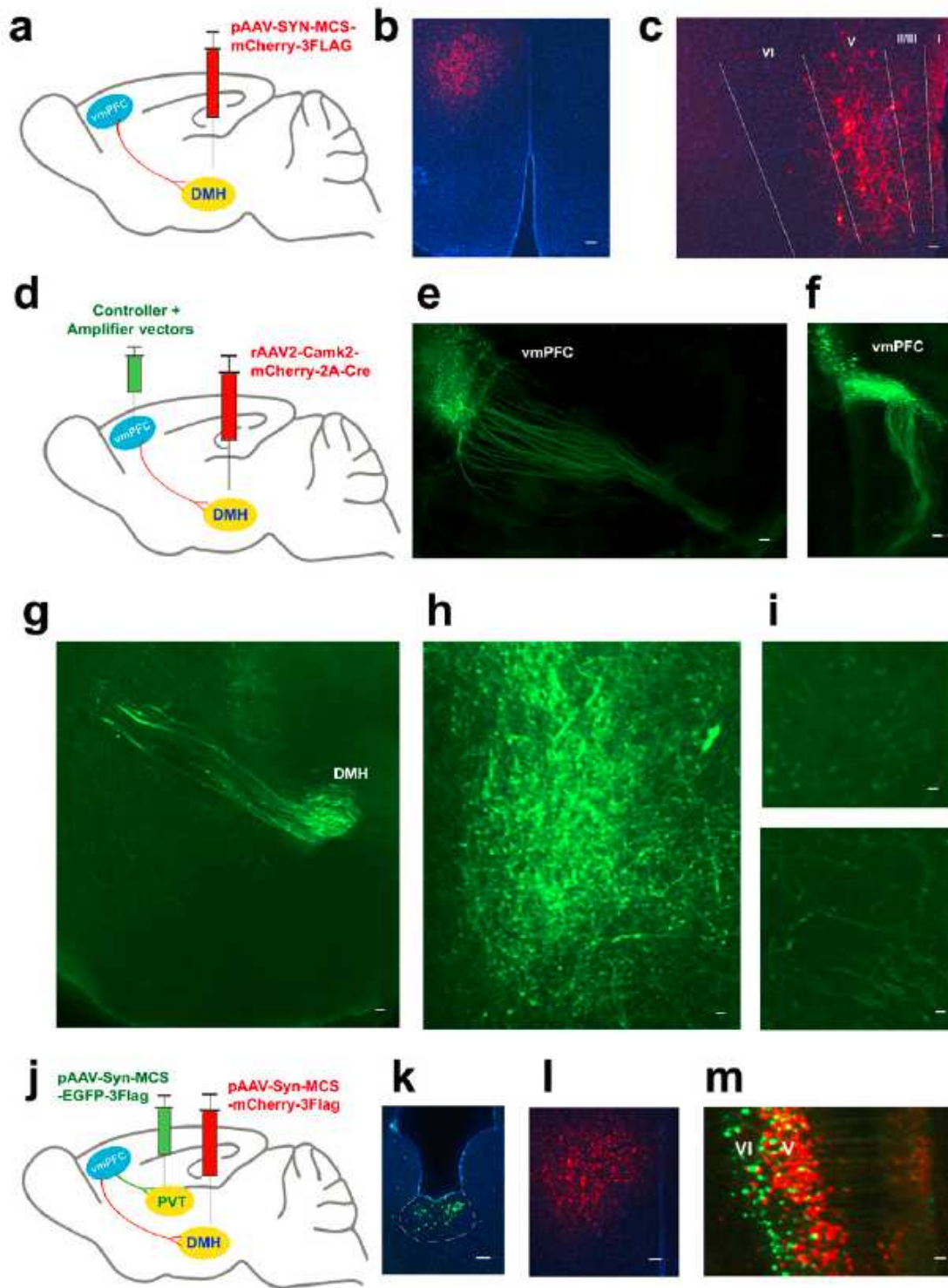
Figure 3

Neuroanatomical tract -tracing of vmPFC -DMH/PVT projections. a,d,j, Schematic sagittal sections show virus or vector injections in theDMH , vmPFC and PVT. b,c, mCherry labeling in the D MH (left) and vmPFC (right). e-i, Sparse labeling of the same vmPFC neurons innervating both the DMH and other brain regions. Sagittal (e and g) and top (f) view sections show EGFP-labeled "mPFC neurons and their axonal projections downward and caudal ward all t he way to terminate in the DMH. Sagittal sections show

EGFP-labeled axons/terminals in the nucleus accumbens (h), bed nuclei of the striaterminalis (i: top) and anterior hypothalamus (i: bottom). k-m, Two viruses injected into the PVT (k: EGFP) and DMH (l: mCherry) are transported back to the vmPFC, where mCherry - and EGFP-labeled cells are distributed mainly in layers V and VL respectively (m). Scale Bars, 400 μm (e and f), 200 μm (b), 150 μm (g), 50 μm (k and l) or 20 μm (c,h,i,m).
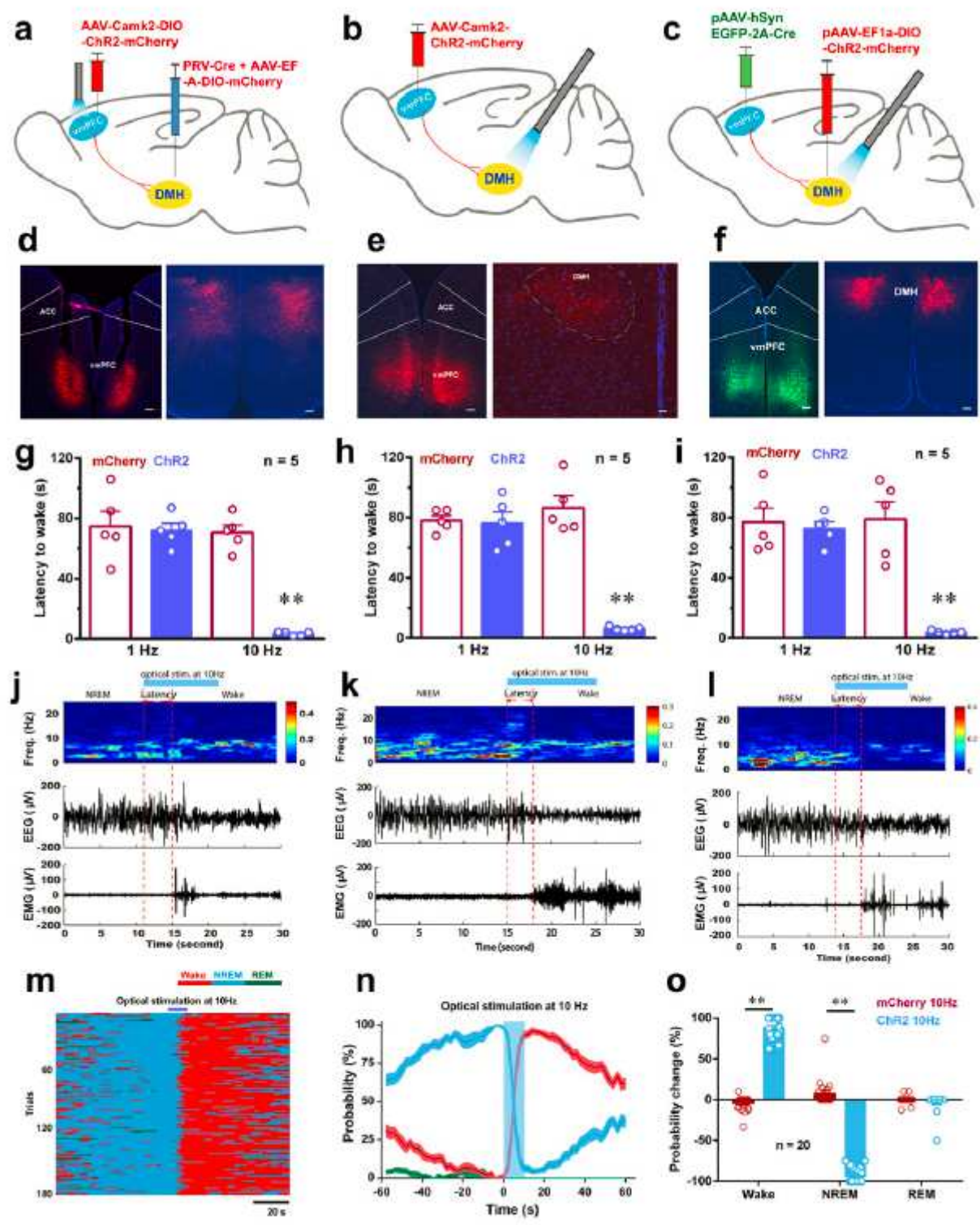

Figure 4

Optoactivation of vmPFC-DMH projections switches NREM sleep to wakefulness. a-c, Schematic sagittal section s show viral injection s into the vmPFC and DMH with optical fiber implantation above the vmPFC (a) orDMH at 40° oralward angle (b and c). d-f, Frontal sections show mCherry- or EGFP-labelling in the vmPFC and DMH. ACC, anterior cingulate cortex. g-i, Latency to wakefulness from NREM sleep by photostimuli. j-1, Representative EEG power spectrum, EEG and EMG traces with color scale indicating the power (m V2) of raw power spectral density. m,n, Brain states in all trials from ChR2-expressing mice (m), and probability of each state around optogenetic stimulation delivered during NREM sleep (n). o, Probability change of each state l 0-s before and during photostimuli. All data are means± SEMs; n = number of mice. ** $p<0.01$ vs. mCherry/1-Hz, Bonferroni post-hoc test after one -way A.NOVA (g: $F_{3,16}$ = 32.2, $p<0.01$; h: $F_{3,16}$ = 44.29, $p<0.01$; i: $F_{3,16}$ = 21.73, $p<0.01$), or** $p<0.01$ vs. mCh /1 0-Hz, Bonferroni post-hoc test after two-way ANOVA (o: $F_{2,16}$ = 638.7, $p<0.01$). Scale bars, 200 μm (d-f: left), 150 μm (f: right), 120 μm (d: right) or 40 μm (e: right).
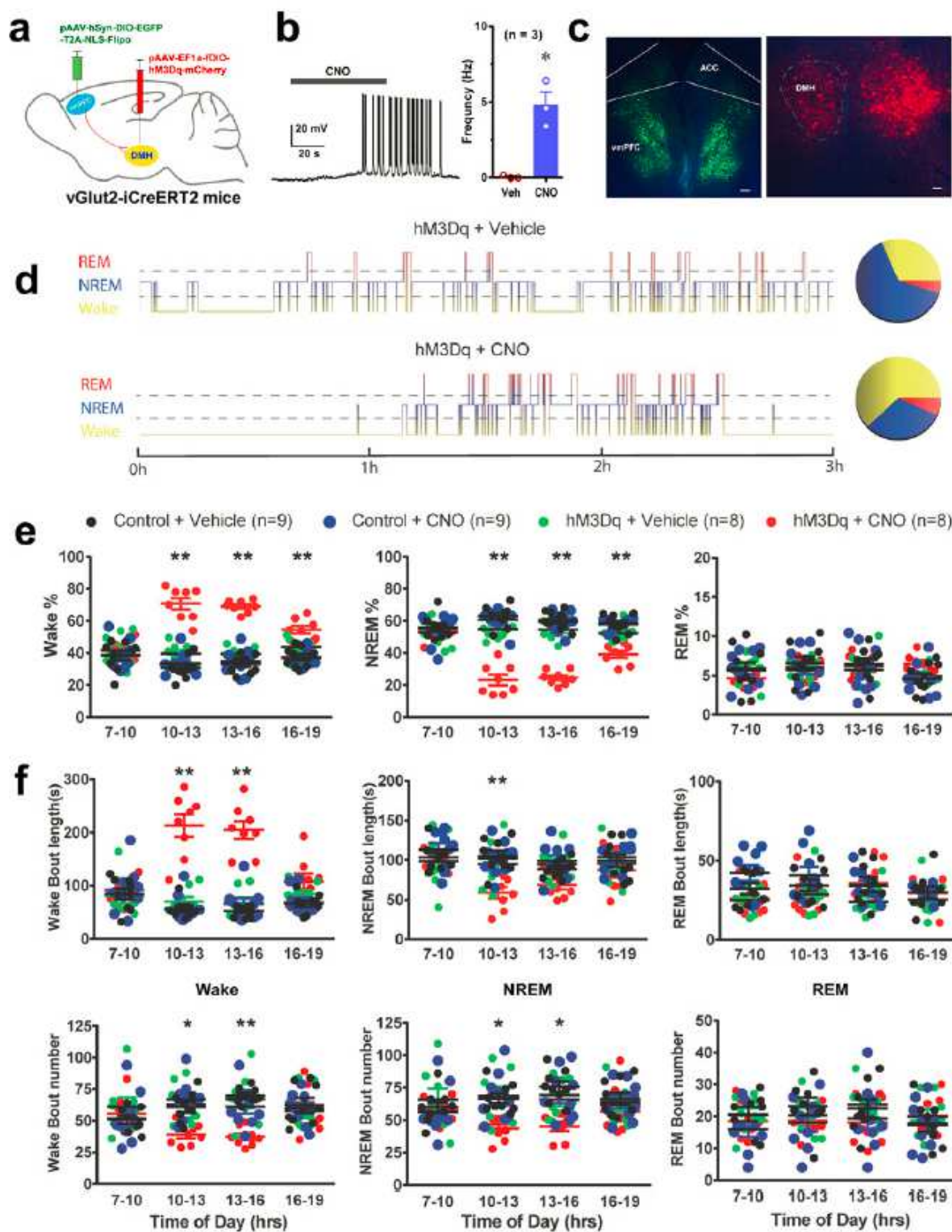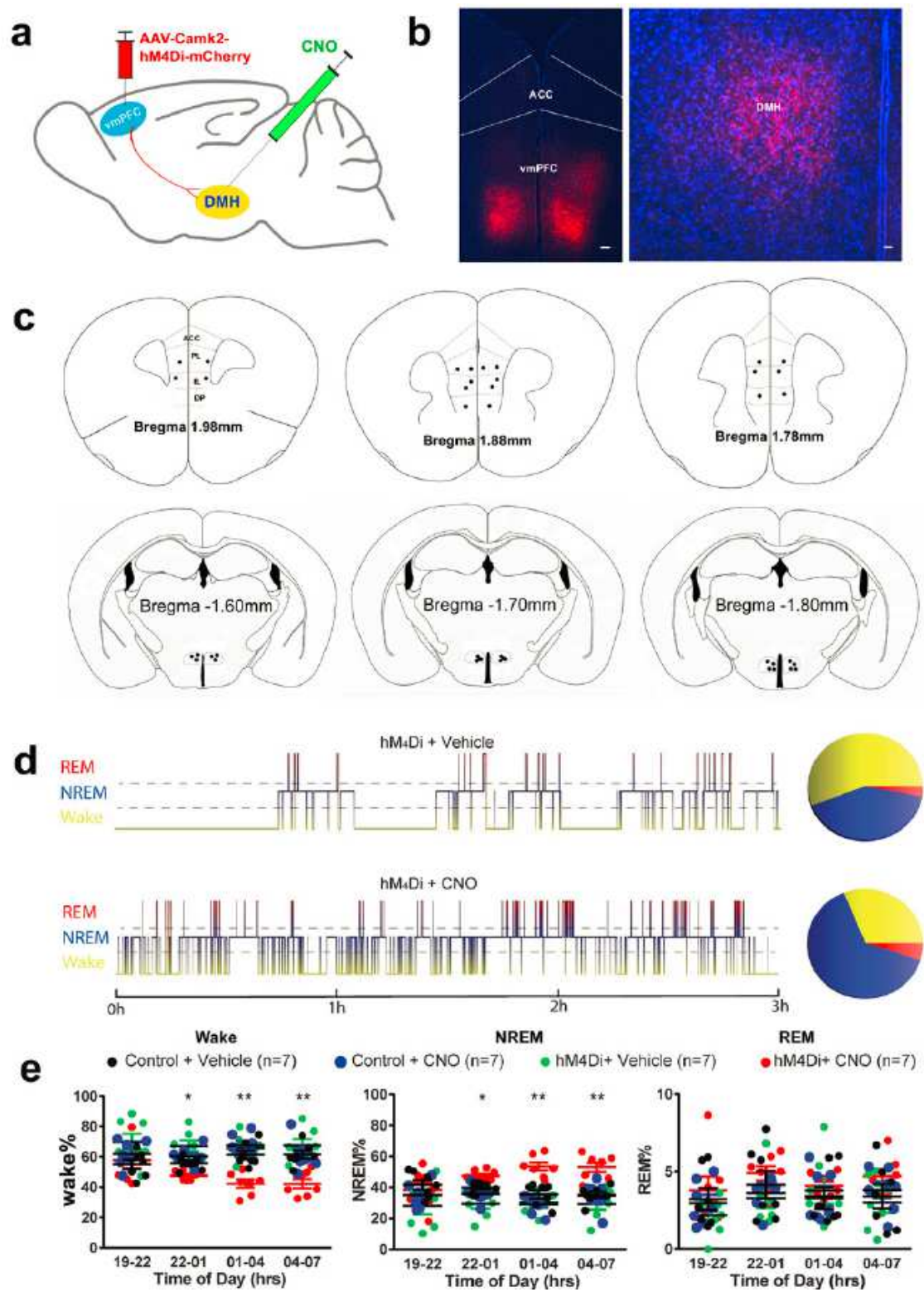
Figure 5

Chemoactivation of DMIB glutamatergic neurons innervated by vmPFCs promotes wakefulness and suppresses NREM sleep. a, Schematic sagittal section show s viral injections in vGlut2 -iCreERT2 mice . b, Increased excitability ofhM3Dq -expressing DMH cells by CNO. c, Frontal sections show EGFP-labeled vmPFC neurons and mCherrylabeled DMH neurons. ACC, anterior cingulate cortex. Scale bars, 200 μm (left) or 40 μm (right). d, Representative 3 -hour hypnogram and pi e chart s. e, Percent of time spent in

different sleep states during light-on period. r, Bout length (top) and number (bottom) of sleep states during light-on period. All data are means:!: SEMs; n = number of mice.* p<0.05 vs. v chicle, Student t-test {b); ** p<0.0 1 vs. control/vehicle, Bonferroni post-hoc test after R.M two-way ANOVA (e: wake%, F3 ;30 = 52.45, p<0.01; :NREM%, F3,30 = 63.21, p<0.01; REM%, F3 ,30 = 0.083,p=0.9688. f: wake length, F3, 30 = 37.29, p<0.01; NREM length, F3, 30 = 3. 157, p<0.05; REM length, F3, 30 = 2.378, p=0.089; wake number, F3 ,30 = 3. 13, p<0.05; NREM number, F3,30 = 3 .167, p<0.05; REM number, F3,30 = 0.704, p=0.557).

Figure 6

Chemoinbibition of vmPFC projections in D:Vffis suppresses wakefulness and promotes NREM sleep a, Schematic sagittal section shows viral injections into vmPFCs with CNO injection into DMHs through a pair of canulae toward DMHs at 40° oralward angle. b, Frontal sections show mCherry -labeled vmPFC neurons and DMH axons/terminals. ACC, anterior cingulate cortex. Scale bars, 200 μm (left) or 20 μm (right). c, Location of central points of AAV-Camk2-hM4Di -mCherry (top) and CNO (bottom) injection sites (black circles) within bilateral vmPFCs or DMHs. CNO injection sites are 1 mm below the cannulae tract tips. DP, dorsal peduncular cortex; IL, infralimbic cortex; PL, prelimbic cortex. d, Representative 3 -hour hypnogram and pie chart. e, Percent of time spent in sleep states during light-off period . All data are means± SEMs; n = number of mice. * $p<0.05$ and ** $p<0.01$ vs. control/vehicle, Bonferroni post-hoc test after RM two -way ANOVA (e: wake%, F_9 ,n = 2.265,$p<0.05$; NREM¾, F_9,n = 2. 564, $p<0.05$; REM%, F_9,n = 0.4237,p=0.9183).
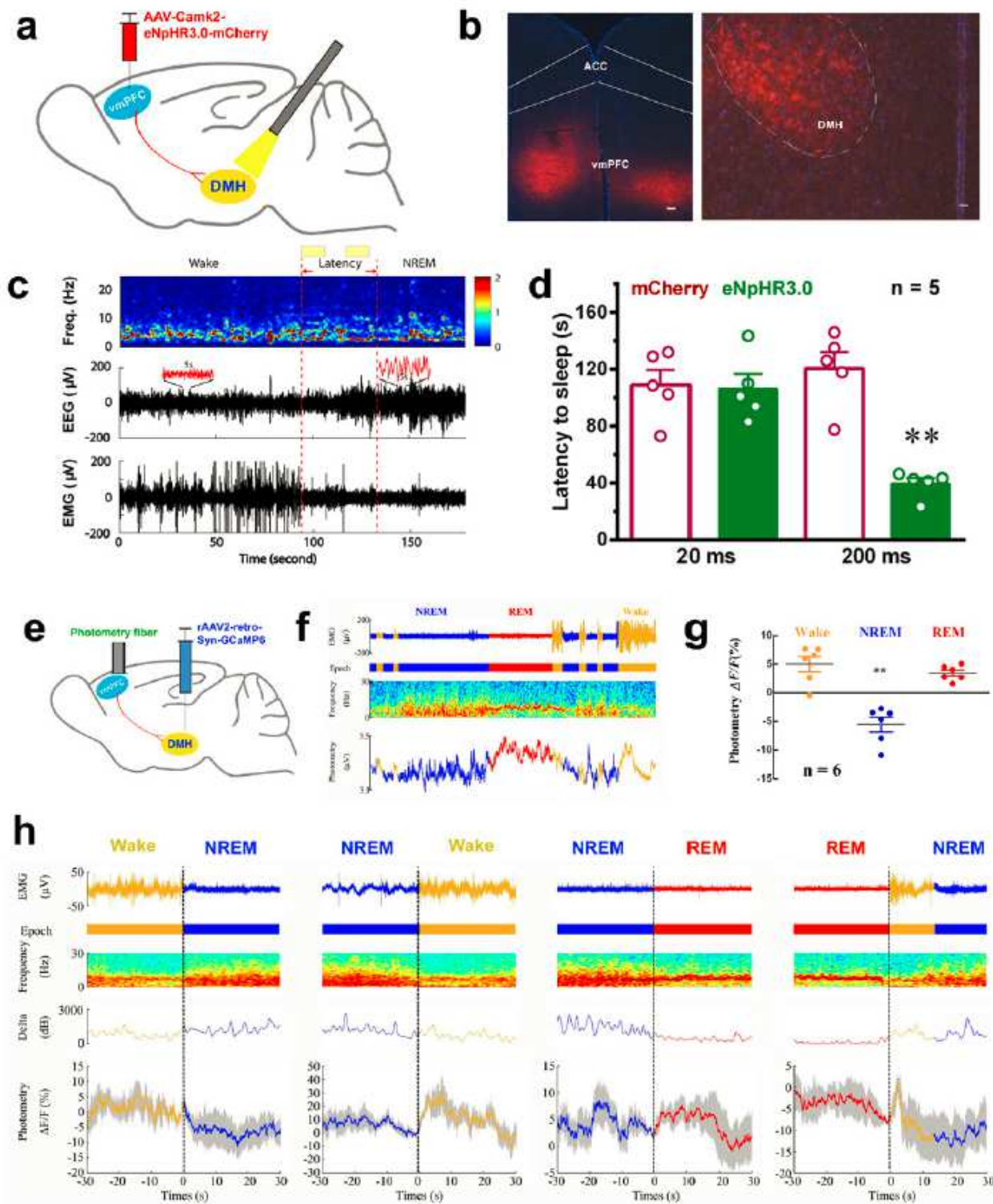
Figure 7

Photoinhibition of m1PFC outputs in D:Vms switches wakefulness to NREM sleep while vmPFC neurons innervating theD:Vm show activity change during sleep-wake cycles. a,e, Schematic sagittal sections show viiral injections into vmPFCs (a) or the DMH (e) with optical fiber insertion above DMHs at 40 ° oral ward angle (a) or photometry fiber detection in the vmPFC (e). b, Frontal sections show mCherry-labeled vmPFC neurons and DMH axons/terminals. Scale bars, 200 μm (left) or 20 μm (right). c, Representative

EEG power spectrum, EEG and EMG traces with color scale indicating the power (mV 2) of raw power spectral density. d, Latency to NREM sleep by photoinhibition. ACC, anterior cingulate cortex. f,h, Changes ofEMG, EEG and mPFC Ca2- signal at a continuous transition (f) or phase to phase transition (h) during sleep -wake cycle with epoch indicating wake (yell ow), NREM sleep (blue) and REM sleep (red). g, delta F/F ratios of the Ca l- photometry signal in the "l>mPFC show inhibition of vmPFC neurons innervating the DMH during NREM sleep and activation during wakefulness and REM sleep . All data are means:!:: SEMs; n = number of mice. ** p<0.0 I vs. mCherry/20 ms, wake or REM, Bonferroni posi-hoc test after one-way ANOVA: Fi 3,16 = 14.49, p<0.01; g: F2,1s = 27.8, p<0.01).
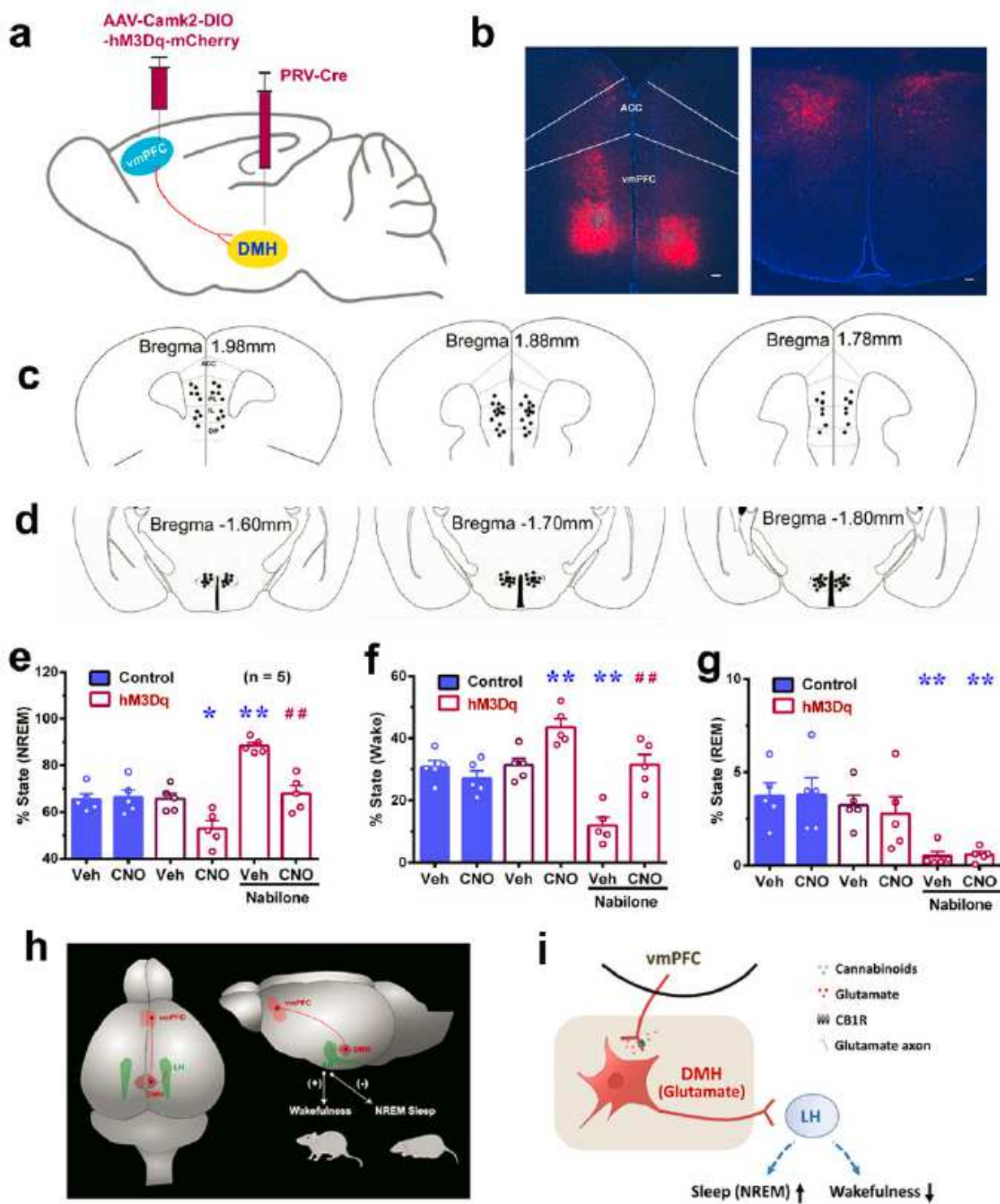
Figure 8

Blockade of cannabinoid effects on NREM sleep and wakefulness by chemoactivation of vmPFC neurons innervating DMHs , and diagrams of vmPFC -DMH-LH promotion for wakefulness and cannabinoid promotion for :\'REM sleep . a, Schematic sagittal section shows viral injection in the vmPFC and DMH . b, Frontal sections show mCherry -labeled vmPFC neurons and DMH neurons. Scale bars, 200 μm (left) or 180 μm (right). c,d, Location of central points of A.AV-Camk2-DIO-hM3Dq-mCherry (c) and PR V -Cre/A.A.

V-EF- A-DIO-mCherry (d) injection sites (black circles) within bilateral vmPFCs (c) and DMHs (d). ACC, anteri or cingulate cortex; DP, dorsal peduncular cortex; IL, infralimbic cortex; PL, prelimbic cortex. e-g, Effects of an i.p. injection of CNO with or without nabilone (I mg/kg, i.p.) on sleepwake states . b, Top and side views of mouse brains illustrating the "mPFC Gtu_DMW1"-LH circuit, whose activation is not only sufficient to pro mote wakefulness and suppress NREM sleep but also necessary for normal sleep -wake behavior . i, Cannabinoids promote NREM sleep a nd suppress wakefulness through activation of CB 1R on axonal terminals descending from thevmPFC, subsequent decreased release of glutamate from the terminals, and deactivation (i.e., inhibition) ofDMH glutamarergic neurons innervating the LH. Data are means:!: SEMs; n = number of mice. • p<0.05 and n p<0.01 vs. Veh, = p<0.01 vs. Veh/Nabilone. Bonferronni post-hoe test after one-way ANOVA (e: F5;24 = 31.43, p<0.01; f: F;,2,< = 49.64, p<0.01; g: F524 = 61.05,p<0.0l).

Supplementary Files

This is a list of supplementary files associated with this preprint. Click to download.

- 31Video1Normal.mp4
- 32Video2REM.mp4
- 33Video4Double.mp4
- 34Video3WtoS.mp4
- FiguresS1S10.pdf